Structural and Mechanistic Studies of a Bacterial Reductive Aminase

Krishnan Srinivas

MSc by Research

University of York

Chemistry

August 2022

Abstract

Biocatalytic methods for the catalysis of reductive amination reactions are currently a focus of intense research. One type of prominently researched enzymes are the Reductive Aminases (RedAms), a subset of Imine Reductases (IREDs). These are NADPH-dependent enzymes that catalyse the amination of ketones into an amine product through an imine intermediate. Recent years have seen a large amount of research on the structural and mechanistic properties of RedAms derived from both fungi and bacteria, in order to better understand their mechanisms and to engineer them for improved catalytic properties. In this study, we have focused on a specific bacterial IRED, IR91 from *Kribella flavida*. IR91 is an IRED that features, a tyrosine Y172 as the catalytic residue within the active site, unlike many other IREDs and RedAms, which feature an aspartate residue enabling reductive amination. IR91 displays activity towards bulky ketone substrates, and is therefore an enzyme with potential for the synthesis of model pharmaceutical compounds.

In this study we successfully solved the structure of IR91 both in complex with its cofactor $NADP^+$ and also with with $NADP^+$ and 5-Methoxy-2-Tetralone (5M2T), a bulky ketone substrate. The IR91 structure displayed high similarity to other known IREDs, including the conserved N-terminal Rossman domain, C-terminal helical domain and interdomain helix in the monomer, and the association of two monomers to form the active dimer. Enzyme kinetics were performed on wild-type IR91, as well as a mutant Y172A, and showed that this residue is essential for catalysis. Biotransformation studies, monitored by gas chromatography, showed that IR91 successfully catalyzed the the reductive amination of 2-tetralone with methylamine to give the product *N*-methyl-1,2,3,4-tetrahydro-2-naphthalenamine with a product conversion of 98%.

Table of Contents

Acknowledgements

I thank my supervisor Prof. Gideon Grogan for offering me the opportunity to do this project as well as his consistent support and guidance. I also thank my mentor Amelia Gilio for her consistent support, guidance and suggestions for carrying out my research project.

I would also like to thank Dr Mahima Sharma, for cloning and providing pET28a plasmids of IR91 WT as well as for mutants, with which I was able to carry out this project. I also thank Balázs Progrányi for producing chemical standards of 5-Methoxy-*N*-methyl-1,2,3,4-tetrahydro-2-naphthaleneamine and *N*-methyl-1,2,3,4-tetrahydro-2-naphthalenamine.

Furthermore, I would like to thank the entire York Structural Biology Laboratories (YSBL) support staff for keeping the labs running, allowing for a smooth research experience. Additionally, I would like to thank YSBL and the Grogan Group for their friendly and welcoming support.

Declaration

I declare that this thesis is a presentation of original work and I am the sole author. This work has not previously been presented for an award at this, or any other, University. All sources are acknowledged as References.

List of Figures

List of Tables

1-Introduction

1.1 Reductive Amination

Reductive amination is a chemical reaction that is used to prepare amines from aldehyde or ketone substrates (**Figure 1**).

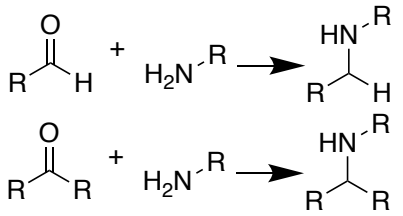

Figure 1- Reductive Amination of Ketones and Aldehydes

In reductive amination, a carbonyl compound and an amine are first reacted together to form an imine intermediate, which is subsequently reduced by a reducing agent such as sodium cyanoborohydride, to give the amine product.[1] Reductive amination has been used to produce biologically active amines used as pharmaceuticals to treat various conditions associated with the central nervous system, cardiovascular, urinary, digestive and respiratory systems.[1] Various amine compounds arising from reductive aminations have also been used to treat cancer, bacterial, fungal and viral infections as well as to regulate metabolic processes.[1] Chiral amines are known to feature as part of the structure up to 40% of pharmaceuticals and have also been used as chiral auxillaries.[2] There have also been notable examples of chiral amine synthesis in the agrochemical and material industries using various organic and transition metal-based catalysts.[3] These have included studies investigating the reactions using cobalt rhodium complexes-based catalysts as well as other group VIII metal-based systems.[4] This is illustrated in **Figure 2**.

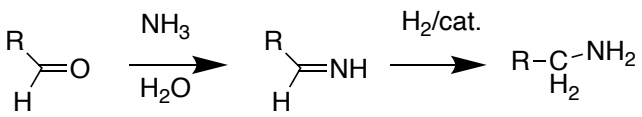

Figure 2- Reductive Amination Reaction scheme using Rhodium-based catalyst

However, most of these 'chemical' reductive aminations have required hazardous reagents and reaction conditions. As a result, biocatalysis, such as enzymatic and biotechnological fermentation processes, have great promise as green and sustainable alternatives.[5] Biocatalysis has also been known to make the synthesis of chemicals a lot easier and thus, a lot of research in this area has been done. Additionally, work in gene mining, directed evolution, recombinant protein production production and enzyme engineering through mutations has enabled many industries to exploit enzymatic reactions, lowering production costs and improving catalytic efficiency.[6-10] More recently, computational studies have also been used to develop more effective catalysts.[11-13]

1.2 Biocatalytic Synthesis of Chiral Amines

One example of an enzyme used in the preparation of chiral amines are lipases, exemplified by the Lipase B from *Candida antarctica* (CAL-B). These lipases can catalyse the enantioselective acylation of racemic amines converting only one enantiomer of a chiral amine, to an acetylated amine and leaving the other enantiomer in high enantiomeric excess. The acetylated amine products can also be subsequently be hydrolysed to give the other enantiomeric amine product.[14] This is illustrated in **Figure 3**.

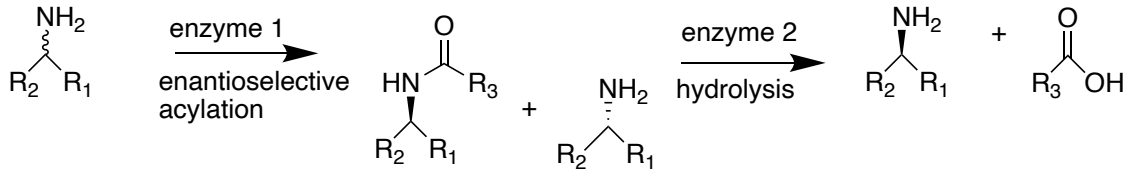

Figure 3- Reaction scheme showing effect of Lipase in producing chiral amines

Lipases can also carry out enzymatic de-acylation, in which a single enantiomer of a racemic amide can be selectively hydrolysed to a chiral amine. Using either of these strategies, it is possible to isolate products with high enantiomeric excess, making it very useful for the manufacture of pharmaceutical amines. [14]

In one example, the selective acylation of (*R*)-1-phenylethylamine from a racemic mixture with ethylmethoxyacetate as the acyl donor produces (*S*)-1-phenylethylamine in an enantiomerically pure form (around 99% e.e.), along with the (*R*)-amide, which can be further transformed to form (*R*)-1-phenylethylamine, through basic hydrolysis.[15-16] This is illustrated in Figure 4.

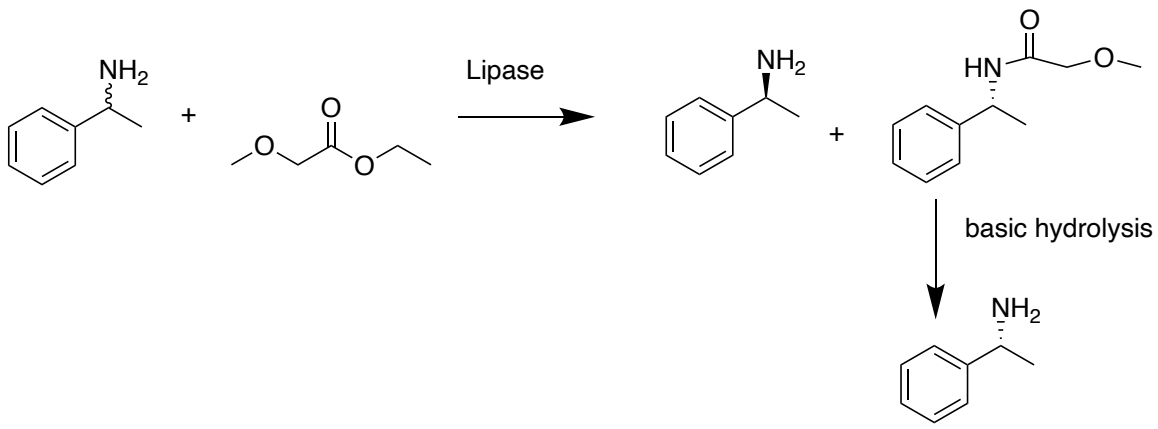

Figure 4- Acylation of phenylethylamine by Lipase

In addition to lipases, extensive research has also been done on ω-transaminases. One of the most prominent examples was in the production of sitagliptin, an antidiabetic drug.[12] More particularly, ω-transaminases have been extensively studied and applied to the synthesis of pharmaceutical compounds like suvorexant, MK-7246 (used to treat helper T-cells), and (*S*)-rivastigmine.[17-20] One of the best characterized ω-transaminases is the -*Cv*-TAm (*Chromobacterium violaceum)*, which has been used to synthesize (*R*)-2,3,4,9-tetrahydro-1*H*-carbazol-3-amine,[21] a precursor for the antiallergic drug ramatroban, used in the treatment of allergic rhinitis.[22] This transaminase was found to synthesise the amine from the ketone precursor in one amination step, as compared to three steps in previous catalytic attempts (including the use of lipases). As a result, the authors managed to improve the yield and produce an enantiopure amine with 96% *e.e*. (**Figure 5**).[22]

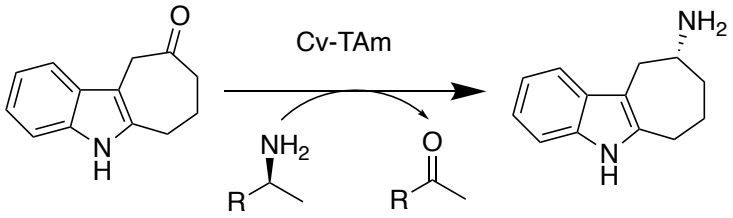

Figure 5- Reaction scheme of the synthesis of (*R*)-2,3,4,9-tetrahydro-1H-carbazol-3-amine, precursor of Ramatroban, catalysed by *Cv*-Tam.

Another well-characterised transaminase is *Pd*-TAm from *Paracoccus denitrificans*, which has been used to synthesize (*S*)-rivastigmine, which is used in the treatment of early stage Alzheimer's disease and also for dementia of Parkinson's patients,[23-24] In this example, the authors managed to improve the yield of (*S*)-rivastigmine {(*S*)-3-[1-(dimethylamino)-ethylphenyl ethyl (methyl)carbamate} synthesis, through a highly stereoselective chemo-enzymatic and shorter synthesis pathway.[23] Furthermore, using *Pd*-TAm as a template, several sequence homology searches and activity guided approaches were conducted to discover several new enzymes.[25] The transaminases described above are superior to lipases largely because they neither require complex sequential operations, wherein intermediates become prone to racemisation nor multiple crystallization steps which involve diastereomeric salts.[21] However, a significant drawback for both transaminases and lipases is that product range only restricted to primary amines.[26-27]

Another enzyme that has been applied to the synthesis of chiral amines are the mono amine oxidases (MAO), including the enzyme from *Aspergillus niger* (MAO-N), which catalyze the conversion of amines to imines. Turner *et. al.* discovered a novel deracemization method to prepare optically active chiral amines, whereby these enzymes oxidise amines into chiral imines and using a recycling system are reconverted to amines, and subsequent further non-selective reduction to chiral amines. These repeated cycles of enantioselective oxidation will increase the yield of chiral amines.[24] MAO-N variants were produced through directed evolution and have been applied to deracemize primary, secondary and tertiary amines.[28-31]As a result, these enzymes can be applied to a broad scope of amines, unlike lipases and transaminases. One example of this is the enantioselective transformation of

pyrrolidines reported by Kohler *et al.* in 2010, developed and applied to amino nitrile synthesis as well as the synthesis of nonproteinogenic amino acids. The process involved an enantioselective oxidation of pyrrolidine followed by a diastereoselective addition at 98% e.e.[32] This is illustrated below in **Figure 6**.

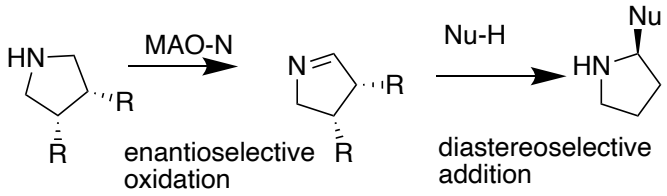

Figure 6- Reaction showing the use of monoamine oxidase in an oxidation-addition cascade reaction

These pyrrolidines are useful in applications in the synthesis of protease inhibitors like telaprevir and bocepevir, which are used in treating hepatitis C virus.[33-34]

Another MAO is the cyclohexylamine oxidase (CHAO), derived from *Brevibacterium oxydans*. This enzyme is able to catalyze the transformation of substrates such as primary amines, alkyl aryl amines and alpha-carbon substituted amines, to produce enantiomerically pure (*R*)-amines with high yields ranging from 62-75%.[35]

1.3 Imine Reductases

Imine Reductases (IREDs) are a new class of biocatalysts, which were first shown to catalyze the asymmetric reduction of performed cyclic imines, giving a range of chiral amine products.[36-38] These enzymes are Nicotinamide Adenine Dinucleotide Phosphate (NADPH)-dependent enzymes that can catalyse the imine reduction reactions from imines to produce chiral amines.[39] More specifically, the enzymes are chemo and stereoselective, giving a diverse range of α-chiral and β-chiral products.[37]

Initially, Stephens *et al.* had done a combinatorial screen using only anaerobic bacterium, *Acetobacterium woodii*, to investigate imine reductase activity, in an attempt to synthesize α-chiral amines.[40] This was because aerobic bacterium and facultative anaerobes are known to likely hydrolyse the C=N bond in imines than reduce it, and hence imine hydrogenation is unlikely to occur in oxidative metabolic

process. The authors used a range of alkyl and aryl components, whilst targeting the reduction of aldimines as part of the screen. These included several bulky imines as well, making them useful to serve as model compounds for pharmaceutical applications.[40]

Along with imine reduction to an amine (**Figure 7A**), IREDs are also able to catalyse the reductive amination of carbonyl compounds, such as ketones or chiral aldehydes with nucleophilic amines provided in large excess, using nicotinamide adenine dinucleotide phosphate (NADPH) as cofactor, to produce secondary amine products.[41-42] **Figure 7B** shows the reactions of IREDs with imines or ketones and amine donors to form secondary amines.

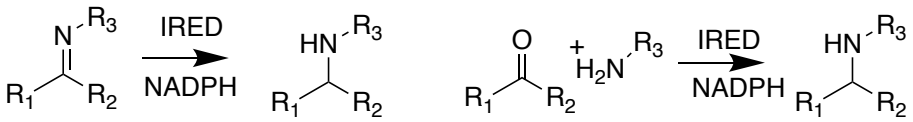

A **B**

Figure 7- **A**) Reduction of an Imine with an IRED, **B**) Reductive amination of a ketone with and amine with an IRED. Both reactions produce secondary amines.

Additionally, many studies have involved engineering IREDs through point mutation or mutagenesis, in order to apply them to the scaled-up synthesis of amines, eventually making them useful for industrial applications.[10]

1.3.1 Structure

The first IRED was discovered from the purification and characterization studies of the IRED from *Streptomyces* done by Mitsukara *et al.*, whereby it was found to be a homodimer consisting of 32kDa subunits.[43] Following this, structural studies have been done on the IREDs by Rodriguez-Mata *et al.* in a native form as well as in complex with NADPH cofactor. The findings indicated that typical IREDs function as dimers, whereby the monomers consist of an N-terminal Rossman-fold attached to a helical C-terminal domain. The dimer is formed by domain sharing whereby the C-terminal is swapped with a substrate binding cleft between the N-terminal of one monomer and the C-terminal of the other monomer.[44] This is shown in **Figure 8.**

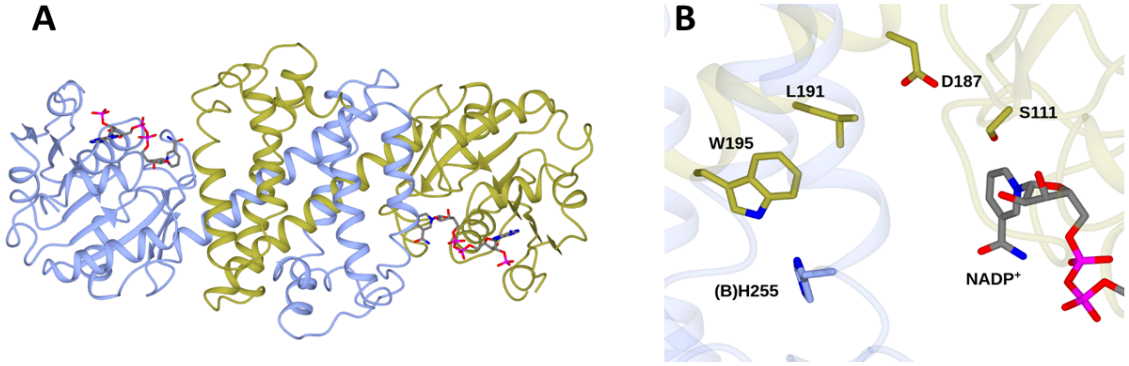

Figure 8- Imine Reductase (IRED) PDB: 3ZHB solved by Rodriguez-Mata *et al.* **A**) dimer showing interlinking domain sharing. **B**) Active site residues in complex with $NADP^+$ cofactor.

More studies found that The Rossman-fold N-terminal domain contains the conserved NADPH-binding domain, made up of 6-parallel beta strands. Unlike the N-terminal domain, the C-terminal helical domain is variable and is used for substrate specificity.[45] Moreover, they are found to be connected by a long inter-domain alpha helix.[39] Further structural studies on some fungal RedAms, also showed vast similarities to the first solved structure, amidst subtle differences in active site residues.[37]

1.3.2 Mechanism

Imines are reduced by hydride delivery from NADPH. It was then initially assumed that protonation occurs at the catalytic site. [44] Based on the first X-ray crystal structure solved and published by Grogan *et al.*, it was suggested that D187 (aspartic acid residue at 187 position) was important for the imine reductase activity as a proton donor. The position of D187 can be seen in the Rodriguez-Mata *et al.* structure shown in **Figure 8B**.[37] A suggested mechanism for reduction and protonation is shown in **Figure 9**.

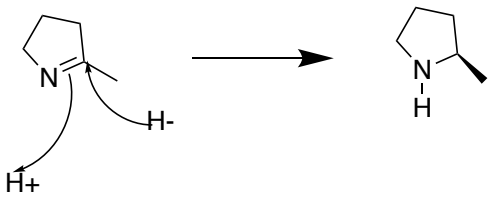

Figure 9- Proposed Mechanism of Imine Reduction by am IRED with H- from NADPH and H^+ from an aspartic acid residue.

1.4 Reductive Aminases (RedAms)

As part of the extensive research done on IREDs, a certain subset of these enzymes are able to convert carbonyl compounds such as ketones into imines and further into amines, when the amine is provided in a ration of 1:1 with the ketone. In these cases, the enzyme appears to catalyze both imine formation and imine reduction. These subsets of enzymes have been named as Reductive Aminases (RedAms). Huber *et al.* were the first to show that IREDs can enable the reductive amination of ketones to an (*S*)-amine, through an imine intermediate. The authors carried out reactions using a bulky ketone such as 4-phenyl-2-butanone with methylamine to produce 2-(methylamino)-4-phenylbutane. However, there yields were low and a large (12.5x) excess of amine was required to drive the reaction, suggesting that this enzyme operated only in an IRED mode.[46] Subsequently, Scheller *et. al.* showed that the IREDs could enable thereductive amination of benzaldehyde and acetophenone to their respective amines occurred with high enantiosselectivity,.[47] Through these initial studies it was established that the major advantage of IREDs over transaminases in reductive amination was that they could catalyze the formation of secondary amines. This property is also not possessed by amine dehydrogenases (AmDHs), which can only convert ketones to primary amines using ammonia as the amine donor.[46]

In certain cases, IREDs were shown to catalyze secondary amine formation using ketones and amine substrates, in a ratio of as low as 1:1, making them inherently relevant from a sustainability standpoint.[48] The subset of IREDs catalyzing this reaction were given the term 'Reductive Aminases' (RedAms) as they were thought to employ a mechanism for the catalysis of both imine formation and imine reduction,

distinct from IREDs, which catalyze only the reduction of imines recruited from solution..[48]

Mechanistic studies on certain RedAms in Fungi such as *Asp*RedAm*, Ad*RedAm *and At*RedAm reported by Sharma *et al.*, suggested that Aspartate-169 (D169) is involved in deprotonating the amine substrate as a nucleophile, which will subsequently attack the carbonyl and produce a carbinolamine intermediate.[49] The intermediate is then dehydrated to an imine, then reduced by a hydride that is transferred from NADPH.[50] This is shown below in **Figure 10**. From further structural and mechanistic studies on fungal RedAms done by Aleku *et al.,* it was found that the mechanism involved three conserved amino acid residues arranged in a catalytic triad-asparagine, aspartate and tyrosine.[48]

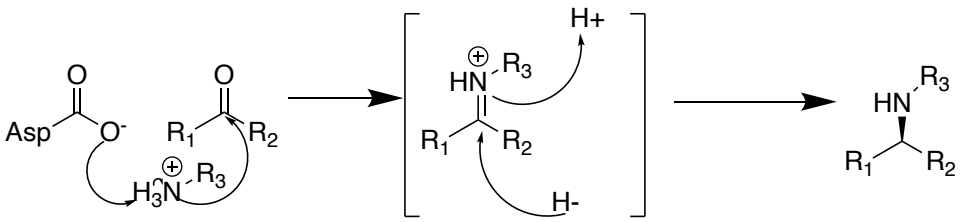

Figure 10- Mechanism of Reductive Aminase with H^- from NADPH

Structural studies of thermotolerant fungal RedAms by Mangaz-Sanchez *et al.* indicated that these enzymes also have the conserved residues of asparagine, aspartate and tyrosine. The authors had solved a 2.25 Å structure that does resemble many features of a typical IRED-family, such as being in a homodimer form with an N-terminal Rossman fold and C-terminal helical bundle by a long alpha helix.[37]

1.5 Previous Work

Along with fungal RedAms, a lot of work has been done to study the use of bacterial IREDs in catalysing reductive amination. France *et al.* selected and sequenced a group of 45 bacterial IREDs that catalyze reductive amination reactions.[51]

Of those, some of them were previously known and some were novel enzymes. Their findings indicated that certain bacterial IREDs such as IR91, from *Kribbella flavida*, which despite significantly different active site residues are able to carry out reductive amination with certain ketones and amines. Following sequential alignment done and subsequent overlay of active site residues in this study, it was found that IR91 had a tyrosine residue Y172 instead of the conserved aspartate amongst the other IREDs tested, and other different residues in the active site, including a leucine L180 instead of tyrosine, and two methionines M243 and M244 instead of a tryptophan and a glutamine.[51]

Additionally, IR91 showed (*S*)-selectivity in the reductive amination of 2-hexanone, 4-phenyl-2-butanone and 2-tetralone with methylamine, giving products with up to 98% enantiomeric excess. [51] A reaction scheme showing the reductive amination of 2-tetralone with methylamine by IR91 is shown in **Figure 11**.

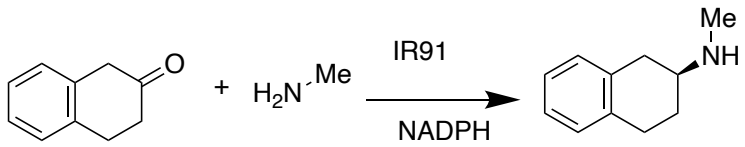

Figure 11- Reaction of 2-tetralone and methylamine, catalyzed by IR91 and NADPH, giving an (*S*)-amine.

Previous examples of a bacterial IREDs with tyrosine in the active site included enzymes from *Streptomyces* sp. 3546 (3546-IRED) and *Narcodiopsis halophila* (NhIRED). In these studies, the authors showed that the enzymes carried out reductions of 2-methylpyrroline (2MPN) to give the (*S*)-amine product. They also provided structural evidence for the importance of the tyrosine residue in the mechanism of imine reduction, as mutation of this residue to an alanine resulted in an enzyme of very porr activity. Man and coworkers solved the structures of the tyrosine IREDs from *Narcodiopsis* and *Bacillus* (PDB codes 4D3S and 4D3F), illustrating the binding of the NADPH cofactor and location of active site residues that may be important for catalysis.[52]

Further work was done by researchers in GlaxoSmith Kline (GSK), which involved expanding the substrate scope of reductive amination activity of different set of IREDs, by using bulky amine donors such as benzene-1-4-diamine with cyclohexanone.[53]

1.6 Aims and Objectives

The identification of IR91 as an interesting enzyme for the transformation of larger ketone substrates prompted us to investigate this enzyme from a structural and mechanistic perspective. This would provide the first information on the structural determinants of reductive amination in an (*S*)-selective tyrosine-containing IRED.

The main objective of this project therefore was to carry out a mechanistic and structural characterization of the wild-type IRED IR91. This was to be achieved through:

- Expression and purification of IR91 to confirm its ability to catalyse the reductive amination of 2-tetralone and cyclohexanone with partner amines such as methylamine .
- Crystallization of wild-type IR91 in complex with NADP+ cofactor and ketone ligands.
- Expression and purification of IR91 mutants Y172A and S97A enabling the determination of effects of mutations of these residues on enzyme kinetics and activity.
- Applying IR91 to the scalable synthesis of model compounds.

2- Experimental

2.1- Gene Sequence

CATATGCCGCCAACCGACCGTACCCCGGTTACCCTGATCG
GTCTGGGTCCGATGGGTCAGGCGATGACCCGTGCGCTGCTGGCGG
CGGGTCACCCGGTGACCGTTTGGAACCGTACCCCGGCGCGTGCGG
CGGGTGTGGTTGCGGATGGTGCGGTGCTGGCGGCGAGCCCGGTGG
AGGCGGTTGAAGCGGGTGATCTGGTTATTCTGAGCCTGACCGATT
ACCAAGCGATGTATGACGTGCTGGAGCCGGCGACCGGTAGCCTGG
CGGGTCGTACCGTGGTTAACCTGAGCAGCGATACCCCGGACCGTA
CCCGTGCGGCGGCGGATTGGGCGACCGAACACGGTGCGACCTTCC
TGACCGGTGGCGTGATGATCCCGGCGCCGATGGTTGGTACCGAGG
AAGCGTACGTGTACTATAGCGGCCCGGCGGAAGTGTTTGAAAAGC
ACCGTACCACCCTGACCGTGATTGGTGCGCCGCGTTATCTGGGCG
AGGACACCGGTCTGGCGCAGCTGATGTATCAGGCGCAACTGGATG
TTTTCCTGACCACCCTGAGCAGCCTGATGCATGCGACCGCGCTGC
TGGGTACCGCGGGCGTTAGCGCGGCGGAGAGCATGCCGGAACTGA
TCGGTATGCTGCGTACCGTGCCGGCGATGCTGGAGGCGGGTGGCG
AAAACCCGGGTGCGGACATCGATGCGGACAAACACCCGGGTGATC
TGAGCACCATTACCATGATGGGTGCGACCGCGGACCACATTGTTG
GTGCGAGCGAAACCGCGGGTATTGATCTGGCGCTGCCGCGTGCGG
TGCAAGCGCACTATCGTCGTGCGATCGAAAACGGTCACGGTGGCG
ATAACTGGACCCGTATCATTGACGGCATTCGTAGCCCGCGTTAAG
GATCC

Figure 12 Gene encoding IR91 wildtype with 900 base pairs.

A PET28a codon optimized IR91 WT gene and an N-terminal his-tag was used for all protein production and work in this report.

2.2- Bacterial Transformation

25 µL of BL21 DE3 cells mixed in 1.5 µL of DNA containing PET28a plasmid and IR91 gene in a 2 mL Eppendorf and kept on ice for 20 min. Then it was heat shocked at 42^{o}C for 45 s, after which it was immediately kept on ice for 2 min. 1 mL Lysogeny Broth (LB) Media was then added to the Eppendorf and incubated for 1 h at 37^{o}C at 180 rpm. After that, the cells were centrifuged at 6000 rpm for 5 min, producing a cell pellet at the bottom of the media. 900 µL of the media was discarded and the remaining 100 µL was resuspended into the cell pellet and then pipetted and spread onto an agar plate containing the Kanamycin antibiotic. The petri dish was then left overnight at 37^{o}C.

2.3- Overnight Cultures

The following day, four overnight cultures were prepared whereby for each, one colony from the transformation plates was inoculated into a falcon tube containing 10 mL LB media and 10 µL kanamycin (30 mg mL^{-1}). The overnight cultures were then left to grow overnight at 37°C with shaking at 180 rpm.

2.4- Scale up of cultures and protein expression

After the overnight incubation, each 10 mL culture of LB media containing grown cells was inoculated into a 2.5 L shaker flask containing 1 L freshly autoclaved LB Media and 1 mL of kanamycin (30 mg mL^{-1}) and left for 1 h at 37°C. OD_{600} values were then measured. Considering that *E.coli* replicates every 20 min, the cultures were then reincubated to ensure that the values were between the targeted range 0.6-0.8. After reaching the targeted range, each shaker flask was then inoculated with 1 mL of 1 M β-D-1-thiogalactopyranoside (IPTG) to induce expression of the target gene. The shakers were then left overnight at 16°C, with shaking at 180 rpm.

2.5- Plasmid purifications

2 x 2 mL of the overnight cultures were placed in each Eppendorf tube and centrifuged at 13.3k rpm for 30 s. The LB supernatant was then discarded, and 200 µL of resuspension buffer was added and resuspended into the cell pellet. The lysis buffer (400 µL) was then added, inverted for five to six times, and then followed by incubation at room temperature for 1 min. Plasmid neutralization buffer (200 µL) was then added and the tubes were gently inverted to ensure a uniform yellow colour, after which it was incubated for 2 min at room temperature. The solution was then centrifuged at 13.3 krpm for 5 min. The supernatant was then transferred to a spin column, followed by a 1 min centrifugation at 13.3 krpm. The flow through was discarded and then 200 µL of wash Buffer I was then added to the filtrate section of the spin column and centrifuged for 1 min, followed by centrifugation with 400 µL Wash Buffer II. The flow through was then discarded and 50 µL of pure water (50°C) was added directly to the membrane and incubated for 5 min and then centrifuged for 13.3

krpm for another five minutes. A nanodrop UV-spectrometer was then used to record the concentrations of the purified plasmids and one of the two samples was sent for sequencing to verify the plasmid.

2.6- Protein purification

Following overnight expression, the cultures were then ultracentrifuged for 20 min at 5 k rpm. The cell pellet was then resuspended into around 25 mL of Buffer A (pH 7.5 containing 500mM Tris, and 30 mM NaCl). The cells were then disrupted at 5^{o}C and at 26.5 kPSi. The disrupted cells were then ultracentrifuged for 40 min at 15 krpm. The cell lysate was then loaded on a Nickel column, allowing the target protein, containing the His-tag, to bind to the Nickel. Using the AKTA machine, a pump wash was done with the Buffer A and the Buffer B (pH 7.5 containing 500mM Tris, 30 mM NaCl, 300 mM Imidazole), The Nickel column containing the protein was then wired into the machine and run for elution.

2.7- SDS Gel Electrophoresis

Each sample contained 5 µL intended fractions, 2 µL of loading dye and 8 µL of pure water. Fractions included insoluble fraction (cell debris after the second centrifuged), cell lysate, flow through after running the Nickel column, and the 25 mL fraction from the AKTA machine. Post elution, fractions containing a peak were collected and each fraction was added separately into the 15 µL sample. Each 15 µL was then loaded onto the well.

2.7.1- Resolving Gel

12% resolving gel was made by mixing 3.2 mL ultrapure deionized water, 2.5 mL resolving gel buffer (1.5M TRIS pH 8.8, 0.4% SDS), 4.2 mL Acrylamide Stock, 50 µL 10% APS and 8 µL TEMED. The resulting mixture was then immediately poured to the gel mould to set for 30 min.

2.7.2- Stacking Gel

Following the setting of the resolving gel, stacking gel was made by mixing 3.2 mL ultrapure deionized water, 1.3 mL Stacking gel buffer (0.5M TRIS pH 6.8, 0.4% SDS), 0.5 mL acrylamide stock, 10 µL Bromophenol Blue, 25 µL of 10% APS and 8 µL TEMED. The resulting mixture was then immediately poured into the gel mould on top of the resolving gel and a comb was added to form wells. The gel was then left to set for 30 min.

2.7.3- SDS-page Electrophoresis

To run one gel, 1 L of SDS buffer was prepared. This included 250 mL of running buffer and 10% SDS (500 mL stock- 125 mL in ultrapure deionised water. The buffer was poured into the gel plates. 15 µL of fraction (containing 8 µL water, 2 µL loading dye, 5 µL fraction) was added to each well with one well reserved for the 10-250 µL DNA marker. The gel was then left to run at 200 V for 50 min. Following the run, the gel was removed from the plate and kept in a box with sufficient pure water and then heated for 1 min. Then water was drained and sufficient amount of blue stain was added to the gel and again heated for 1 min. The gel was then left for further staining for 5 min, with slow stirring. After staining, the gel was then briefly observed and bands were identified, following which the gel was destained with ultrapure deionized water overnight.

2.8 Kinetics

Since the IR91 reaction involves NADPH oxidation to NADP+, the rate of oxidation was monitored, by measuring the decrease in absorbance at the indicative wavelength of 340 nm. To obtain kinetic constants of IR91 for cyclohexanone, a reaction included 0-90 mM ketone, 96 mM methylamine from buffer stock adjusted to pH 9, and 0.5 mM NADPH. A similar setup was done to obtain kinetic constants of IR91 for methylamine with a typical reaction mixture consisting of 0-120 mM methylamine, 10 mM cyclohexanone and 0.5 mM NADPH. A graph was plotted using a Cary UV spectrometer at wavelength 340 nm, showing a decrease in absorbance for 2 min, as a measure of activity. Non-linear regression based on Michaelis Menten kinetics was

then used for further data processing to obtain kinetic constants, through the Origin software.

2.9-Biotransformations

In order to obtain analytical data for biotransformation studies, gas chromatography (GC) assays had to be developed. The aim of was to obtain optimal conditions in which two distinct peaks of the ketone and aminated product standard could be observed. These assays were developed for the substrates cyclohexanone, 2-tetralone and 5-methoxy-2-tetralone. Based on the volatility of these compounds, the following conditions were decided to be tested for each ketone:

1. 100-180^{o}C with a ramp rate of 5^{o}C min
2. 100-140^{o}C with a ramp rate of 5^{o}C min^{-1}
3. 140^{o}C isothermal

For each standard, 1 uL each of a 1 mg mL^{-1} solution of the relavant compound(s) (ketone standard, aminated product standard, and a mixture of the ketone and aminated product) was injected.

After, obtaining the conditions for GC analysis, these were then used to carry out biotransformation studies using 1 mg mL^{-1} of pure IR91 protein and the substrates, in order to test for successful reductive amination. Biotransformation studies were carried out using cell lysate and conditions repeated in the France *et al.* study.

Using the cell lysate, containing the IR91 protein, 200 mg mL^{-1} wet cell weight stock solution was diluted to a 3 mL reaction mixture containing pH9 Tris Buffer, NADPH, glucose, Glucose dehydrogenase (GdH), and ketone. The Reaction scheme is shown in **Figure 24**.

Once the amine was added, the start time of the reaction was noted and the mixture was left to incubate with stirring at 25^{o}C, and used to set up reactions for analysis using Gas Chromatography (GC). At several time intervals, 200 µL of the

reaction mixture was taken and quenched with sodium hydroxide (16 µL, 10 M) and ethyl acetate (400 µL), and then centrifuged at 13.3krpm for 1 min, producing an aqueous and organic layer. The organic layer was then isolated, dried with magnesium sulphate ($MgSO_4$), again centrifuged and then kept in a Gas Chromatography (GC) vial. For reactions with methylamine, samples were taken after 0, 1, 2, 4, 6, 8, 23 and 24 h of the reaction taking place. Subsequently, for reactions with *N*-propylamine, samples were taken after 0 and 24h.

2.9 Crystallization

Screening of crystallization conditions was performed using commercially available INDEX (Hampton Research), PACT premier and CSSI/II (Molecular Dimensions) screens in 96-well sitting drop trays.

Crystals of the IR91-NADP+ complex were grown using IR91 concentrated to 15 mg mL^{-1} in mother liquod solution composed of 0.2 M Lithium Sulphate monohydrate, 0.1 M BIS-TRIS, pH 5.5 , 25% w/v polyethylene glycol (PEG 3350). The crystals were grown in a 1:1 ratio between the mother liquor and the protein was solution.

Crystals of the IR91 in complex with $NADP^+$ and 5-methoxy-2-tetralone (5MT) were grown using IR91 concentrated to 11 mg mL^{-1} in 0.2 M ammonium sulphate, 0.1 M BIS-TRIS, pH 5.5, 25% w/v Polyethylene glycol 3350 (PEG 3350)

Crystals were harvested directly into liquid nitrogen with nylon CryoLoops™ (Hampton Research), using mother liquor without any further cryoprotectant.

3. Results and Discussion

In order to investigate the structural and mechanistic properties of the IR91 enzyme, work was done to express and purify the IR91 enzyme, after which the protein would be used to produce crystals and then further build a structure. The purified protein would also be used to carry out enzyme kinetic analysis and biotransformation studies.

IR91 was purified from an expression using a PET28a plasmid in *E. coli* (BL21 DE3) cells using a nickel affinity column, which is able to bind proteins containing a His-tag, which is present in the protein. Following nickel column purification, a size exclusion column (SEC) was done. For both, nickel column and size exclusion column, an SDS-PAGE Gel was run with results shown below in **Figure 13** and **14**.

3.1- SDS-PAGE

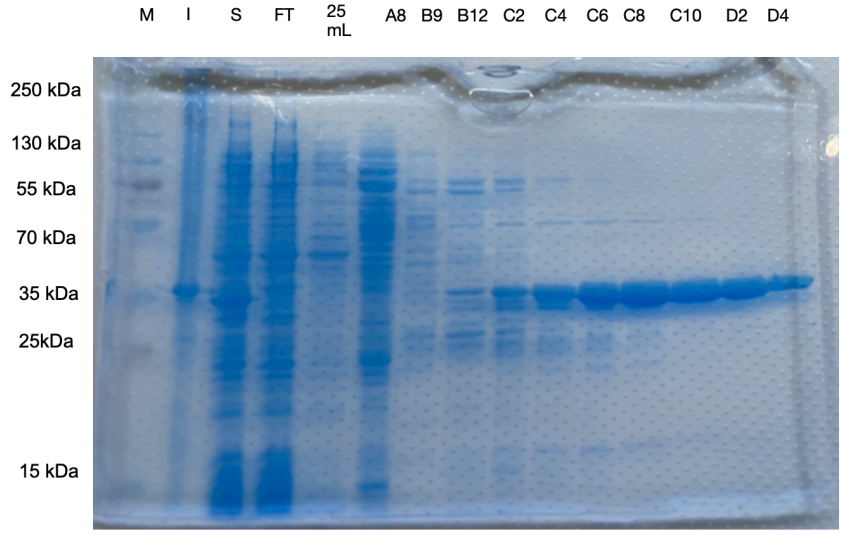

Key
M- Marker, I-Insoluble Fraction, S-Soluble Fraction, FT- Flow through, 25mL- 25mL flow through from AKTA column before elution

Figure 13- SDS-PAGE analysis of IR91 fractions from a nickel column.

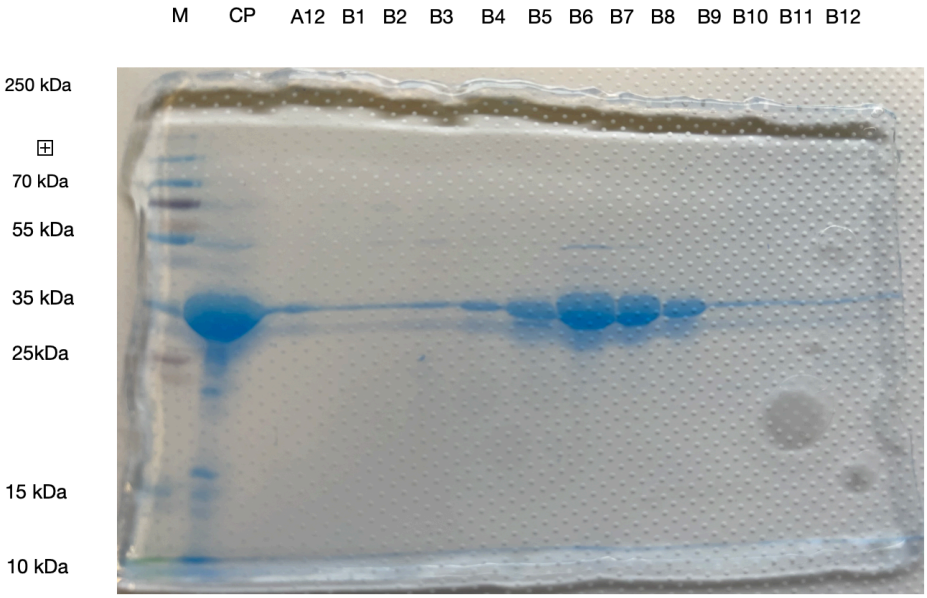

Key
M- Marker 10-250kDa, CP- Concentrated Protein from Nickel fractions C4 to D6

Figure 14- SDS-PAGE analysis of IR91 fractions from a size exclusion column (SEC).

In both of the SDS-PAGE gels, there is a significant amount of a protein present between 25 kDa and 35 kDa, indicating that it is the IR91 protein, since the molecular weight determined using Protparam is 30.8 kDa. This indicates that the IR91 protein has been successfully expressed and purified. Despite a significant amount of protein being indicated in the gel, there was a low yield of protein (100 µL) in the required concentration for crystallization, i.e. 10-15 mg mL^{-1}. As a result, 4 x 1 mL LB cultures were then used in order to scale up the enzyme production. This resulted in protein yields as high as 2 mL at 15 mg mL^{-1}.

Along with successful expression of wild-type, the mutants Y172A and S97A were also successfully purified through nickel column affinity purification and through a size exclusion column. Their successful expression is indicated on the SDS-PAGE shown in **Figure 15**. Both proteins also showed an SDS-PAGE band near 35 kDa after both a nickel column purification and SEC steps, proving the expression of mutants.

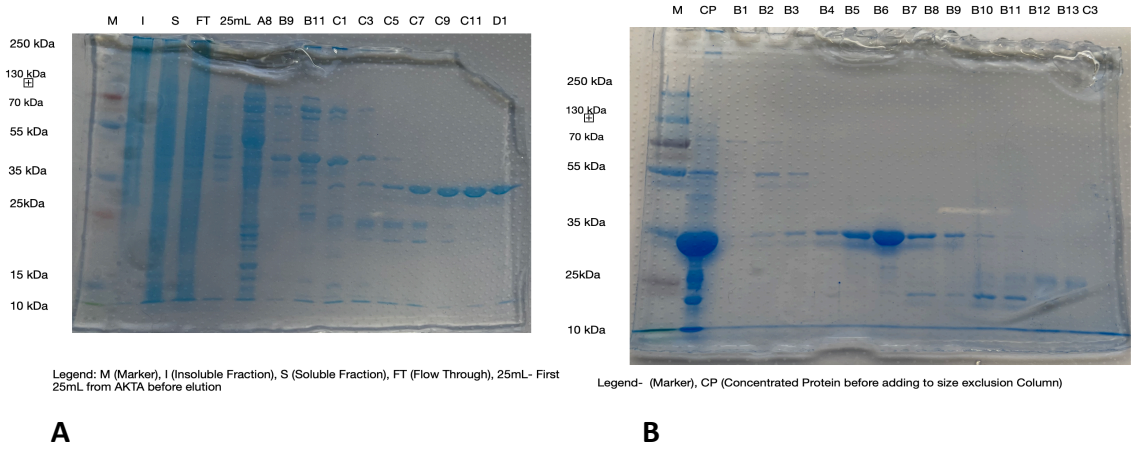

Figure 15- SDS-PAGE of IR91 Y172A mutant **A**) after Ni affinity purification **B**) After a Size exclusion Chromatography (SEC) column).

3.2 Crystals

Using the IR91 wild-type (WT) protein at a concentration of between 10-15 mg mL^{-1}, crystal screens were prepared using Index and PACT trays consisting of protein and NADP+ cofactor. These were done to identify conditions that were optimal for crystal growth. The crystals were then sent to the synchrotron to undergo X-ray diffraction, in order to obtain a dataset. These data sets were then subsequently used to build and refine a structure. These structures will permit a better assessment of the catalytic properties of the enzyme and also possibly help to describe how the substrate and cofactor are binding in order for the enzyme to mechanistically function in the reaction. Since the active site residues are different from other IREDs, it would be interesting to see if and how the substrates bind differently in order to examine the reaction.

After 2 d of setting the screening trays, a large number of crystals was produced, in many conditions especially in the Index screen (**Figure 16**). PACT and CSS screens also had crystals grown in four and one condition respectively. Considering the quality of crystals, Index screens at G2 and G3 were immediately fished and sent to the synchrotron.

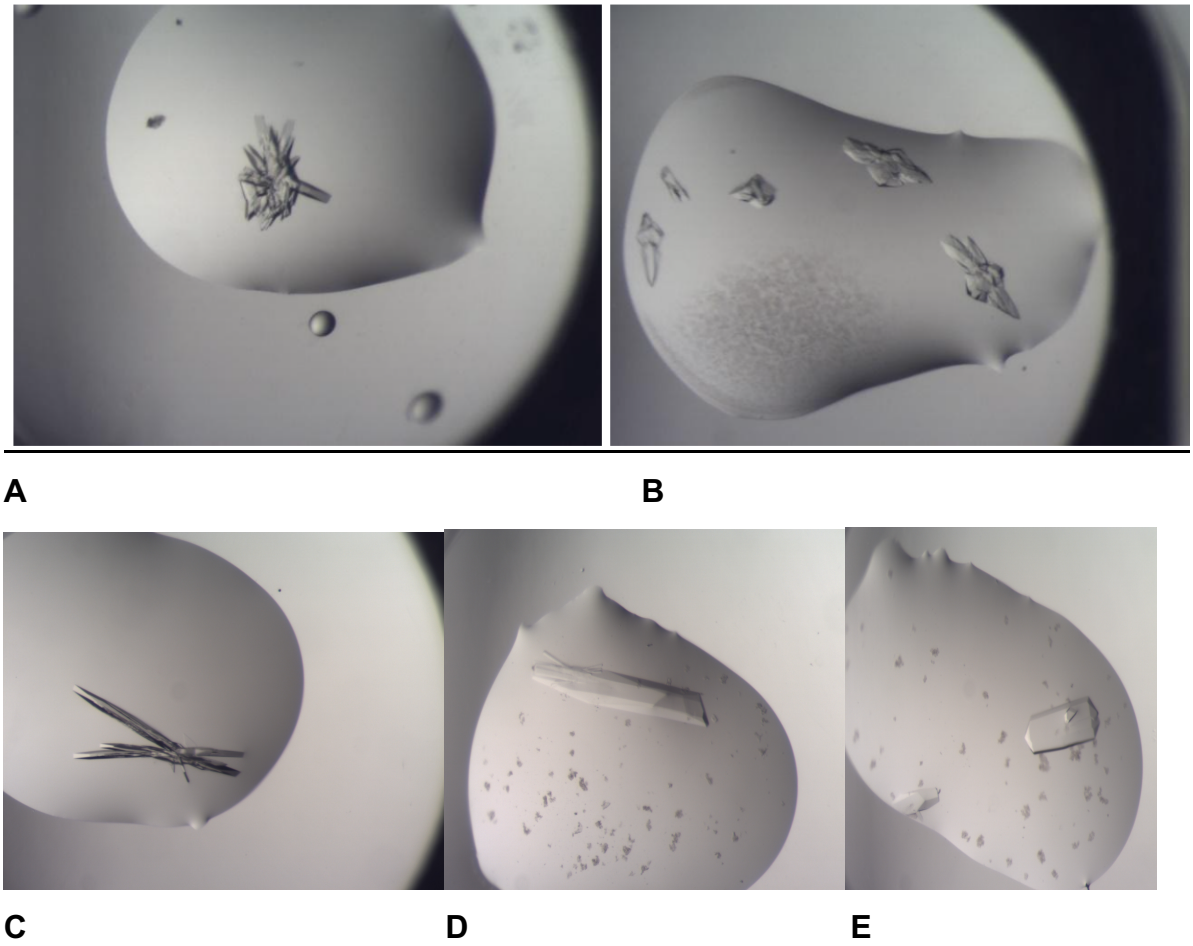

Figure 16- Crystals shown after an INDEX screen **A**) crystals grown in the A5 condition (0.1 M HEPES pH7.5, 2.0 M ammonium sulphate), **B**) crystals grown in the A6 condition (0.1 M Tris pH 8.5, 2.0 M Ammonium sulphate), **C**) crystals grow*n* in A4 condition (0.1M BIS-TRIS pH6.5, 2.0M Ammonium sulfate), **D**) crystals grown in the F12 (0.2 M Sodium chloride, 0.1 M HEPES pH 7.5, 25% w/v Polyethylene glycol 3,350), condition, **E**) crystals grown in H12 (0.15 M potasium bromide, 30% w/v polyethylene glycol monomethyl ether 2,000).

As a result, crystals were formed in the A4, A5, A6, F12 and H12 conditions as shown in **Figure 16**. Unfortunately, there were no crystals formed in any of the PACT screening trays. The H12 and F12 crystals were fished and sent to the synchrotron.

An optimization (48-well) tray was prepared using the A5 conditions with half of the wells containing just protein and cofactor (2 mM) and the rest containing protein,

2 mM cofactor and the 10 mM 2-tetralone ligand (dissolved in DMSO). However, there were no crystals in them and there was a lot of phase separation (largely due to the DMSO). As a consequence, another 48-well tray was prepared with 2-tetralone dissolved in ethanol, but it did not yield any results. As a result, one could conclude that the conditions in the screen were only suited for the protein with cofactor. Following this, new screens were prepared using protein, cofactor (2 mM) and 2-tetralone ligand (dissolved in ethanol) (10 mM), as shown in **Figure 17**.

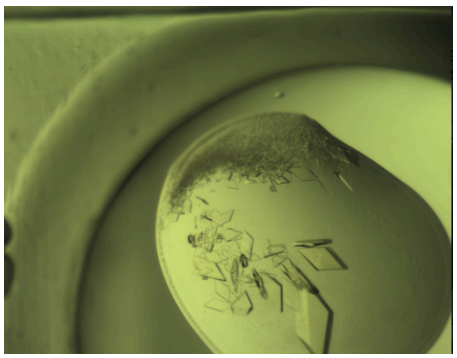

Figure 17 Index screens with ratio 800 nL Mother Liquor: 800nL Protein (bound to cofactor and 2-tetralone ligand G2 condition fished and sent for X-ray crystallography.

After seeing several crystals grow, the crystal grown in the G2 mother liquor (0.2 M Lithium Sulphate monohydrate, 0.1 M BIS-TRIS, pH 5.5 , 25% w/v polyethylene glycol (PEG 3350) were fished and sent to Diamond for data collection.

3.3 Data collection, structure solution and refinement

The datasets described in this report were collected at the Diamond Light Source, Didcot, Oxfordshire, UK on beamline 103. The datasets described in this report were collected at the Diamond Light Source, Didcot, Oxfordshire, U.K. on beamline I03. Data were processed and integrated using XDS[54] and scaled using SCALA[55] included in the Xia2[56] processing system. Data collection statistics are provided in **Tables 1** and **2**. The crystal of IR91-$NADP^+$ was obtained in space group $P2_12_12_1$, with two molecules in the asymmetric unit. The solvent content in the crystals was 48.8%. Crystals of IR91-$NADP^+$-5-MT were obtained in space group

$P2_1$, also with two molecules in the asu. The solvent content in these crystals was 52.1%. The structure of IR91-$NADP^+$ was solved by molecular replacement using MOLREP[57] with the monomer of IRED PDB code 6JIZ) as the model. The finished model was used to solve the structure of IR91-$NADP^+$-5-MT. The structures were built and refined using iterative cycles in Coot[58] and REFMAC,[59] employing local NCS restraints in the refinement cycles. Following building and refinement of the protein and water molecules in each structure complex, residual density was observed in the omit maps at the dimer interfaces, which could be clearly modelled as $NADP^+$. Additionally, further residual density in the IR91-$NADP^+$-5-MT complex could be modelled as 5-MT.

The final structures of IR91-$NADP^+$ and IR91-$NADP^+$-5MT exhibited % R_{cryst} /R_{free} values of 15.4/17.9 and 15.4/18.2 respectively. Refinement statistics for the structures are presented in **Table 1** and **Table 2.** The structures of IR91-$NADP^+$ and IR91-$NADP^+$-5MT will be deposited in the Protein Databank (PDB) prior to submission for publication.

Table 1: Data collection and refinement statistics for IR91 in complex with $NADP^+$. Numbers in brackets refer to data for highest resolution shells.

	IR91-$NADP^+$
Beamline	I03
Wavelength (Å)	0.976246
Resolution (Å)	51.85 – 1.35 (1.37-1.35)
Space Group	$P2_12_12_1$
Unit cell (Å)	a = 51.85, b = 102.55; c = 108.32 α = β = γ = 90.00˚
No. of molecules in the asymmetric unit	2
Unique reflections	117976 (3554)
Completeness (%)	92.9 (57.3)
R_{merge} (%)	0.06 (0.73)
$R_{p.i.m.}$	0.02 (0.32)
Multiplicity	13.4 (11.0)
$\langle I/\sigma(I)\rangle$	21.8 (3.0)

Overall *B* from Wilson plot ($Å_2$)	12
$CC_{1/2}$	1.00 (0.91)
R_{cryst}/ R_{free} (%)	15.4/17.9
r.m.s.d 1-2 bonds (Å)	0.013
r.m.s.d 1-3 angles (°)	1.90
Avge main chain B ($Å^2$)	16
Avge side chain B ($Å^2$)	18
Avge waters B ($Å^2$)	30
Avge $NADP^+$ B ($Å^2$)	11
Avge 5MT B ($Å^2$)	-

3.3.1 Structure of IR91 in complex with cofactor

The structure of IR91 was very similar to the structures or previously determined IREDs, with two monomers forming the active dimer (**Figure 18A**).

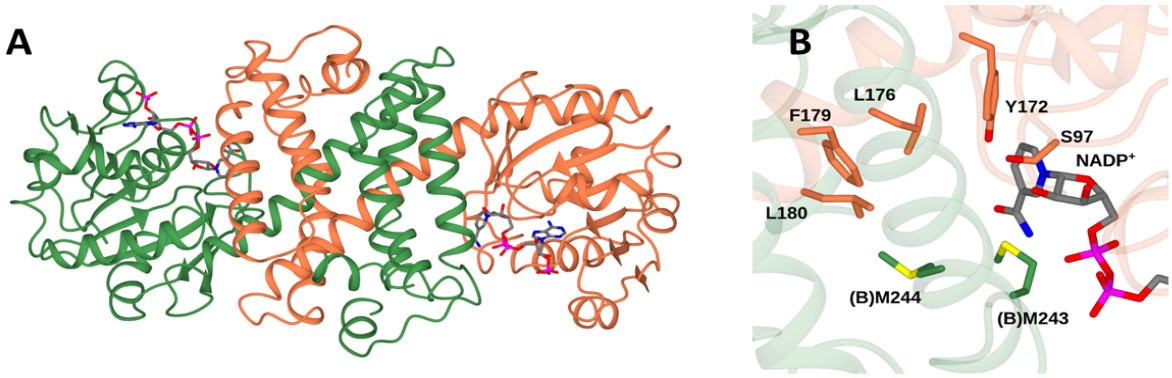

Figure 18- A) Dimer of IR91 with $NADP^+$ cofactor **B**) IR91 active site residues

Figure 18A shows the a dimer, with each monomer displaying an N-terminal fold domain and C-terminal helical domain, as previously found in the first solved structure of an IRED by Rodriguez Mata *et al.* The $NADP^+$ cofactor was found to be within the active site cleft at the dimer interface.[44] Additional residues, such as the catalytic tyrosine Y172 and S97 were observed in the active site, with S97 making an H-bond to the phenolic hydroxyl of Y172. Many hydrophobic residues, including L176, F179,

L180 and M243 and M244 from the neighboring monomer were also observed near the $NADP^+$ cofactor in the active site (**Figure 18B**).

Considering their positions, mutations were decided in order to better study the mechanism of this enzyme. While solving the structure, although some additional electron density was observed in the active site adjacent to the nicotinamide ring of the cofactor, this was not sufficient to build the 2-tetralone ligand. As a result, the crystal trays were again prepared but this time the 2-tetralone concentration was increased from 10 mM to 20 mM. Along with 2-tetralone, screening trays were prepared with 20 mM each of 2-Tetramethylamine, 5-Methoxy-2-Tetralone and 5-Methoxytetramethylamine.

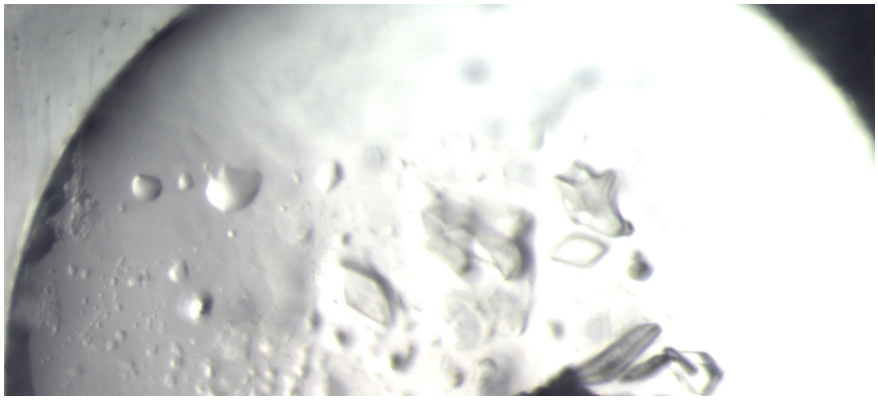

Figure 19- Crystal containing IR91-NADP+ complex with 5-Methoxy-2-Tetralone fished from the F6 (0.2 M ammonium sulphate, 0.1 M BIS-TRIS, pH 5.5, 25% w/v Polyethylene glycol 3350 (PEG 3350) condition with 800 nL Mother Liquor:800 nL protein complex

From the screens carried out, a couple of crystals grew and were fished and sent for X-ray diffraction at the Diamond Light Source (**Figure 19**).The crystal containing the IR91-$NADP^+$ complex with 5-methoxy-2-tetralone (5M2T) complex fished is shown above in Figure 12. Using the same data processing, and structure refinement packages and programmes as described earlier, a structure with the ketone ligand was successfully produced. The data refinement and statistics used to build the structure are shown below in **Table 2.**

Table 2-Data collection and refinement statistics for IR91 in complex with $NADP^+$ and 5-Methoxy-2-tetralone (5M2T). Numbers in brackets refer to data for highest resolution shells.

	IR91-$NADP^+$-5M2T
Beamline	I03
Wavelength (Å)	0.97630
Resolution (Å)	110.00-1.55 (1.58-1.55)
Space Group	$P2_1$
Unit cell (Å)	a = 52.00, b = 110.00; c = 54.00 α = γ = 90.00˚; β = 94.20 ˚
No. of molecules in the asymmetric unit	2
Unique reflections	74559 (1527)
Completeness (%)	85.1 (35.1)
R_{merge} (%)	0.11 (1.14)
$R_{p.i.m.}$	0.04 (0.63)
Multiplicity	6.4 (3.9)
$<I/\sigma(I)>$	13.8 (1.2)
Overall *B* from Wilson plot ($Å_2$)	13
$CC_{1/2}$	0.93 (0.52)
R_{cryst}/ R_{free} (%)	15.4/18.2
r.m.s.d 1-2 bonds (Å)	0.012
r.m.s.d 1-3 angles (°)	1.69
Avge main chain B ($Å^2$)	19
Avge side chain B ($Å^2$)	21
Avge waters B ($Å^2$)	33
Avge $NADP^+$ B ($Å^2$)	15
Avge 5MT B ($Å^2$)	37

3.3.2 Structure of IR91 with cofactor and ligand

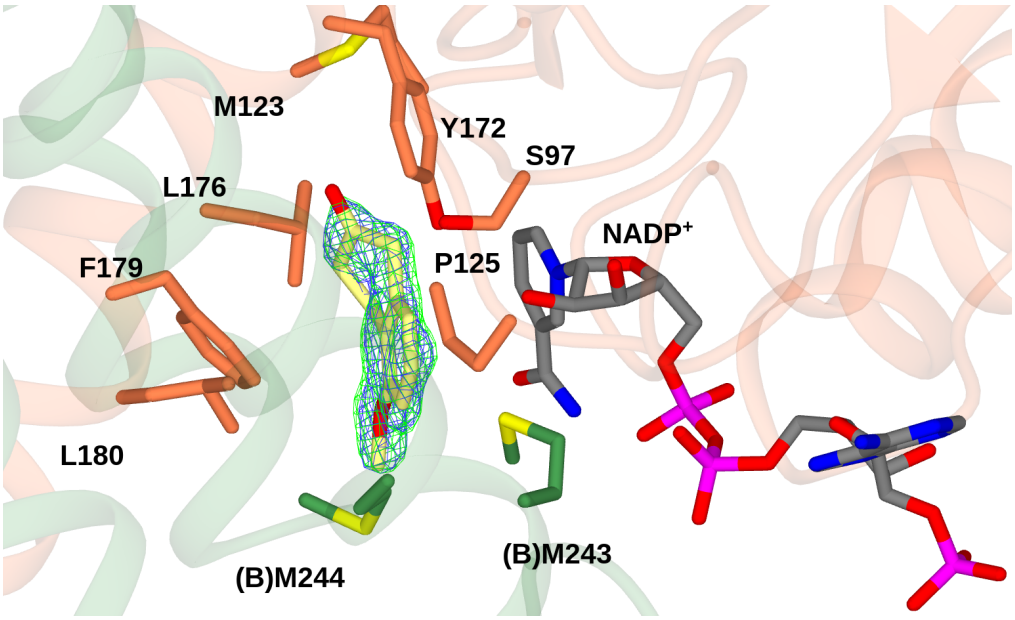

Figure 20- Structure of the IR91 wild-type active site in complex with $NADP^+$ and 5M2T (5-Methoxy-2-Tetralone) with the ligand carbon atoms in yellow. The electron density corresponds to the $2F_o$-F_c and F_o-F_c maps in blue and green and at levels **1s** of and 3**s** respectively. The maps are those obtained prior to refinement of the ligand. Ligand atoms have been added for clarity.

Having successfully produced the ligand bound structure, one can see the way the active site of the enzyme interacts with the 5-Methoxy-2-tetralone (5M2T) ligand and the $NADP^+$ cofactor ligand. The $NADP^+$ cofactor is positioned within the active site cleft near residues of S97, M243, P125 and Y172. The 5M2T ligand is positioned between the nicotinamide ring of the NADP cofactor and the aromatic ring of the phenylalanine 179. The carbonyl group of the ligand is positioned towards the back of the active site as shown, approximately 5.1 Å from the side chain phenolic hydroxyl of Y172. Additionally, the methionine residues at M243 and M244 and the leucines at L176 and L180 provide a hydrophobic environment for the binding of the ligand.

3.4 Kinetics

Kinetic studies were performed to assess the catalytic properties of IR91. 340 nm is the diagnostic wavelength for NADPH.[60] **Figure 21** shows a Michaelis Menten plot for cyclohexanone with IR91, obtained through non-linear regression analysis.

The reactions consisted of cyclohexanone (from 0-90 mM) reacting with 96 mM methylamine, catalysed by 0.2 mg mL^{-1} of wild-type IR91, as shown.

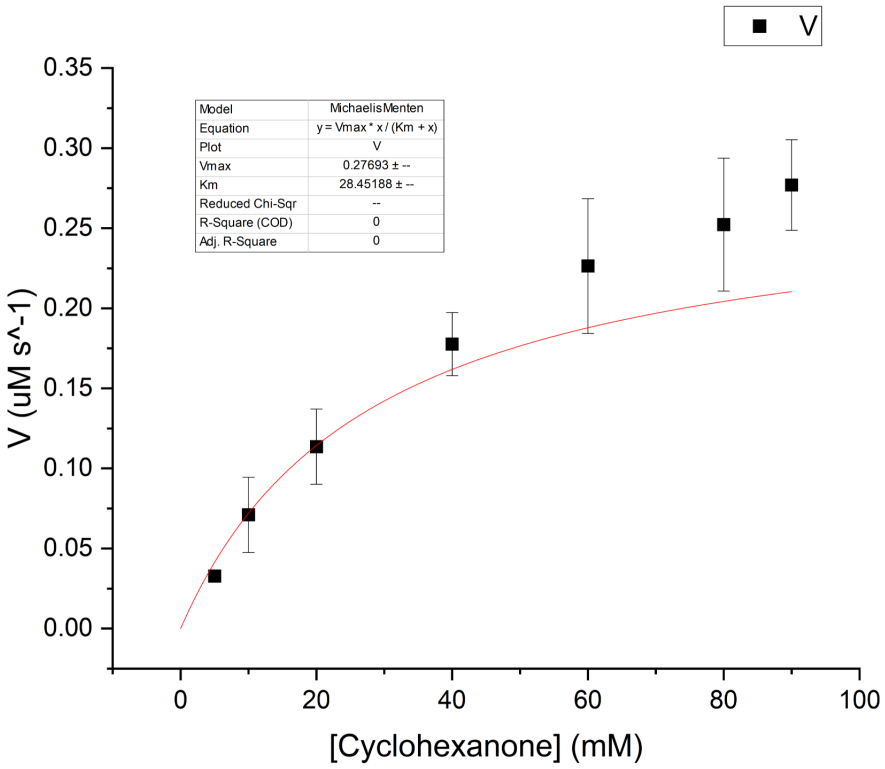

Figure 21- Cyclohexanone kinetics Michaelis Menten plot using 0.2 mg mL^{-1} WT protein.

Seeing that the Michaelis Menten curve could not plateau enough to get a V_{max} value, 0.1 mg mL^{-1} of enzyme was used instead, resulting in the plot shown in **Figure 22**.

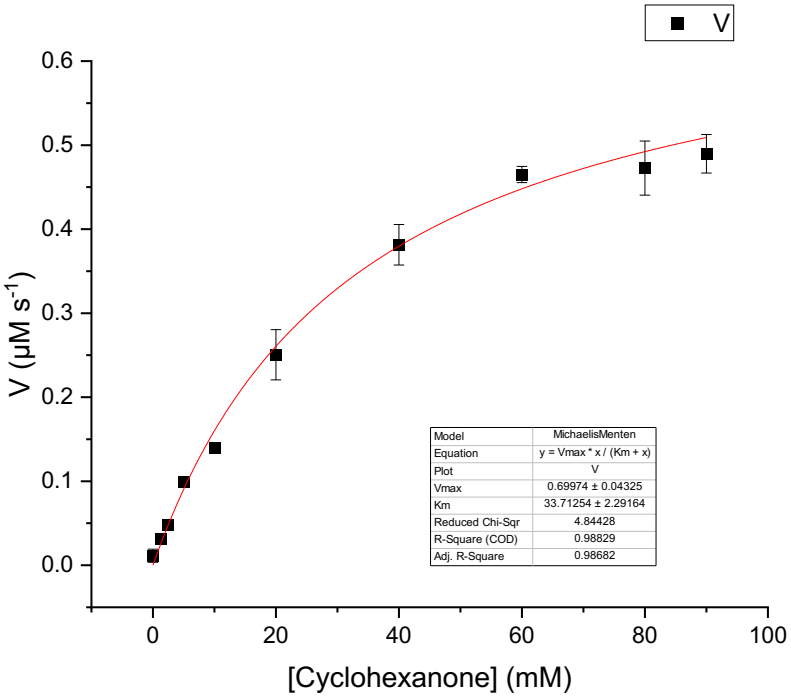

Figure 22- Cyclohexanone Kinetics Michaelis Menten plot with 0.1 mg mL^{-1} IR91 protein.

The graph formed a better plateau, producing a K_m value of 33.71 mM and a V_{max} of 0.69 μM s^{-1}. Amine kinetics was then done with different serial dilutions of the methyl amine (0-120 mM) with constant cyclohexanone concentration (10 mM), catalysed by 0.1 mg mL^{-1} IR91 enzyme. The resulting Michaelis Menten plot is shown below in **Figure 23**.

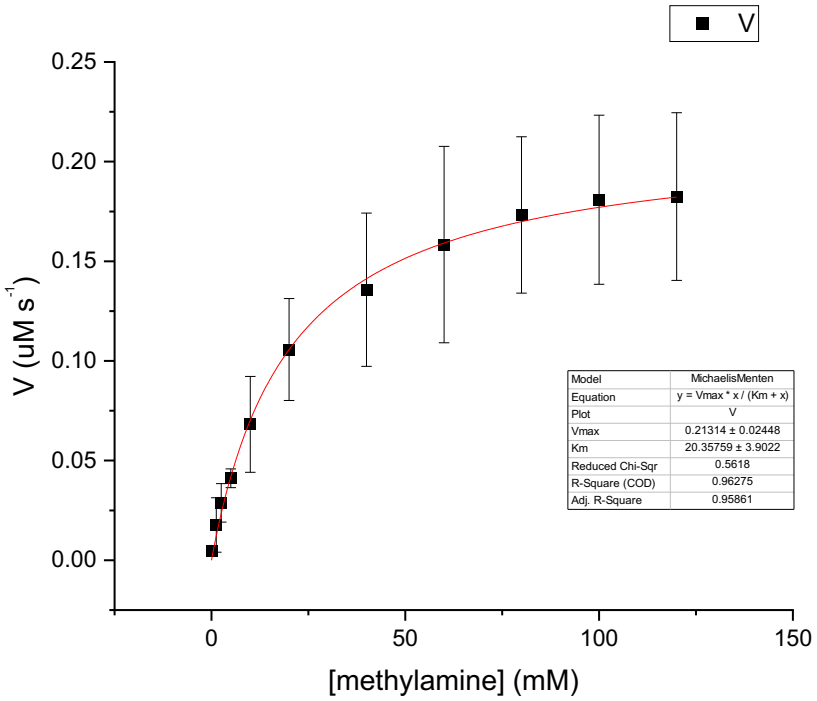

Figure 23- Amine Kinetics Michaelis Menten plot with 0.1 mg mL^{-1} IR91 protein.

As a result, a K_M value of 20.35 mM and V_{max} of 0.21 μM s^{-1} for reactions were obtained with methylamine kinetics. These measurements served as a benchmark for mutant analysis.

With regard to mutant analysis, the data was quite difficult to obtain. For both Y172A and S97A, there was not a clear plateau and the velocity, which was very low, at each concentration did not show any clear trend. This perhaps suggests that the tyrosine residue Y172A and serine S97A are crucial to the mechanism. The structures when considered with the inactivity of the mutants suggest a possible role for Y172 and S97A in catalysis.

3.5- Biotransformations

Using the WT-IR91 cell lysates obtained after cell disruption, biotransformations were done with 2-tetralone and methylamine in the presence of the enzyme (present in the lysate), NADP+ cofactor as well as a recycling system of glucose and glucose dehydrogenase. The reactions were done using the method

previously reported by France *et al.* These were being replicated with 2-tetralone and methylamine in order to compare values with the France *et al.* study. The reaction scheme is shown in **Figure 24**.

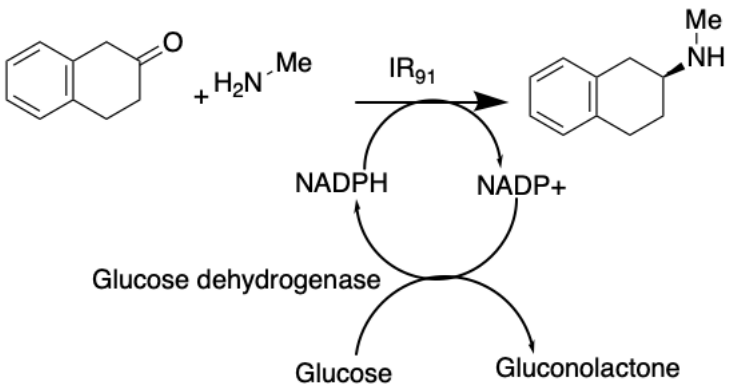

Figure 24- Biotransformations with tetralone and methylamine and cofactor recycling system

3.5.1 Assay Development

In order to obtain analytical data for biotransformation studies, an assay had to be developed, which involved experimenting several different Gas Chromatography (GC) conditions. The aim of was to obtain optimal conditions that produced two distinctive and resolute peaks indicating the ketone and the aminated product. This would be useful as a baseline for reactions done with with 2-tetralone and 5-Methoxy-2-Tetralone. These are large bulky compounds useful to serve as model compounds. The following figures from **Figure 25** to **Figure 27** show assays done under different temperature GC conditions to identify the suitable condition for biotransformation studies involving 2-tetralone.

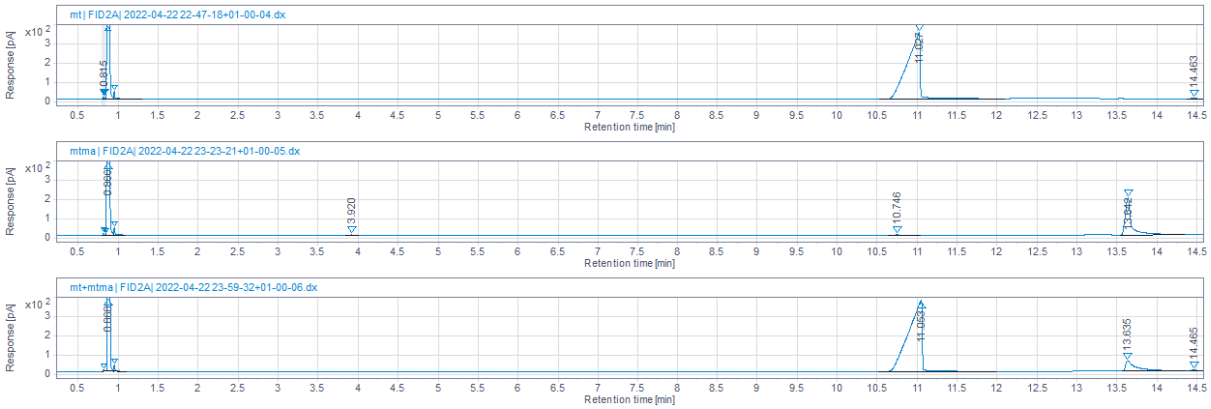

Figure 25- GC traces of 1)- 2-tetralone, 2) *N*-methyl-1,2,3,4-tetrahydro-2-naphthalenamine standard, 3) mixture of tetralone and *N*-methyl-1,2,3,4-tetrahydro-2-naphthalenamine standard in conditions of 100-140ºC with a ramp rate of 5ºC per min.

Figure 25 shows that the 2-tetralone alone eluted at 11.0 min, the aminated product alone eluted at around 13.5 min. When both the ketone and aminated product were mixed in sample, they eluted respectively at 11.0 and 13.5 min. In all the tests, the peak shown before 1.0 min is that of the ethyl acetate solvent.

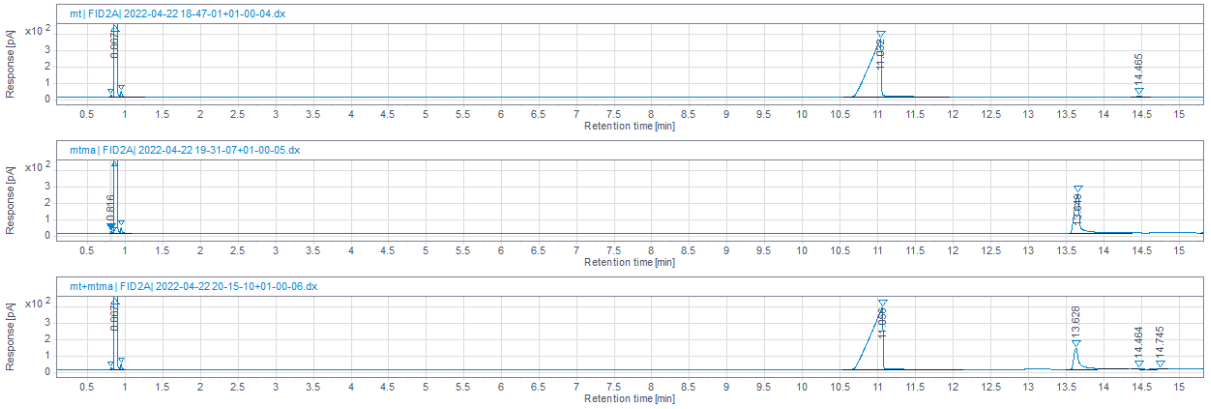

Figure 26- GC traces of 1)- 2-tetralone, 2) *N*-methyl-1,2,3,4-tetrahydro-2-naphthalenamine standard, 3) mixture of tetralone and *N*-methyl-1,2,3,4-tetrahydro-2-naphthalenamine standard in conditions of 100-180ºC with a ramp rate of 5ºC per min.

Figure 26 shows the tests done at temperature conditions between 100-180ºC. It shows that the 2-tetralone alone eluted at 11.0 min, the aminated product alone eluted at 13 min and a mixture of the ketone and product resulted in peaks at 11 min and 13 min respectively.

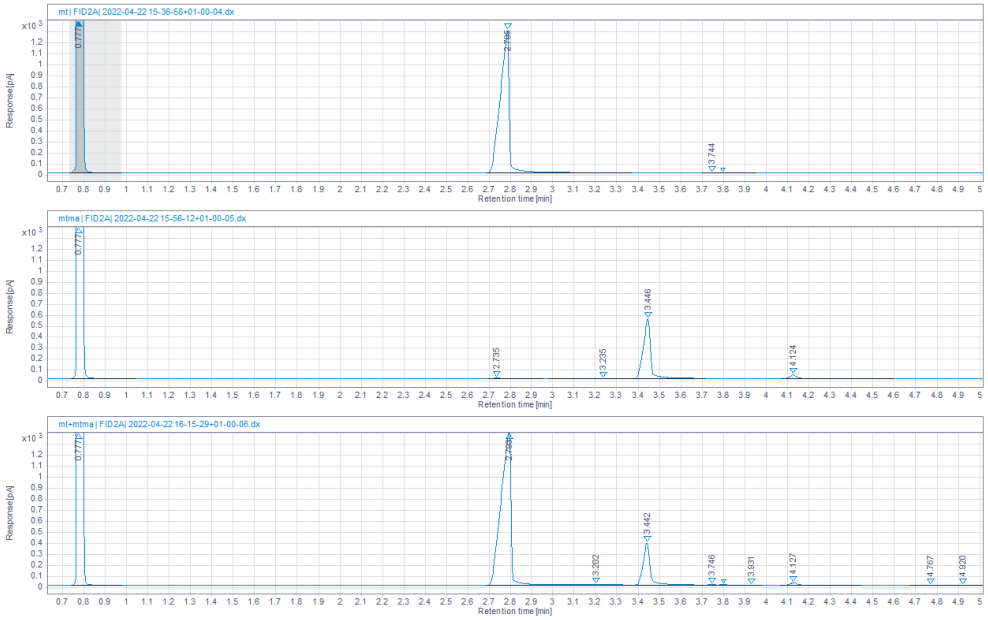

Figure 27- GC traces of 1)- 2-tetralone, 2) *N*-Methyl-1,2,3,4-tetrahydronaphthalen-2-amine standard, 3) mixture of 2-tetralone and methylamine in conditions of 140^{o}C isothermal.

Figure 27 shows the GC traces done with an isothermal at 140^{o}C. In a sample of 2-tetralone alone, a prominent peak was eluted at 2.8 min, whereas with the aminated product standard alone, there was a peak at 3.4 min and a finally, a mixture of the two produced peaks at around 2.9 min and 3.7 min. Based on these GC traces, all of the conditions produced separate product and reactant (ketone) peaks with good resolution. However, it was decided that further biotransformation studies involving 2-tetralone woulduse an isothermal method at 140^{o}C. This was because the peaks eluted relatively quickly and both the ketone and product eluted before 5 min.

Assay development was similarly done for the 5-Methoxy-2-tetralone substrate as well as the aminated product standard under three different temperature gradient conditions. The traces of each temperature condition are shown below in **Figures 28-30.**

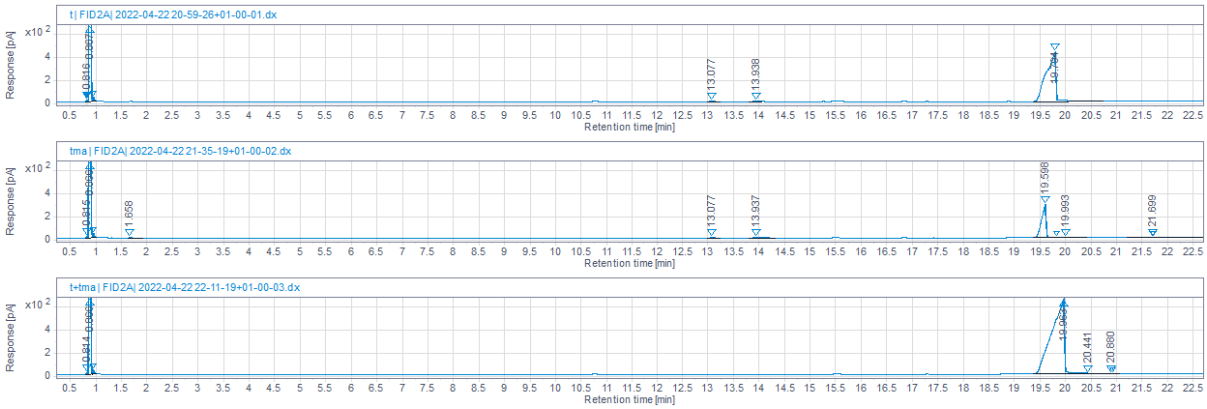

Figure 28- GC traces of 1)- 5-Methoxy-2-tetralone, 2) 5-Methoxy-*N*-methyl-1,2,3,4-tetrahydro-2-naphthaleneamine standard, 3) mixture of 5-methoxy-2-tetralone and 5-Methoxy-*N*-methyl-1,2,3,4-tetrahydro-2-naphthaleneamine with each sample run under in conditions of 100-140^{o}C with a ramp rate of 5^{o}C per min.

Figure 28 shows that at a temperature gradient between 100-140^{o}C, the 5-methoxy-2-tetralone and the aminated product both eluted at around 7 min. As a result, a sample containing the mixture of the product and reactant could not produce separate and resolute peaks.

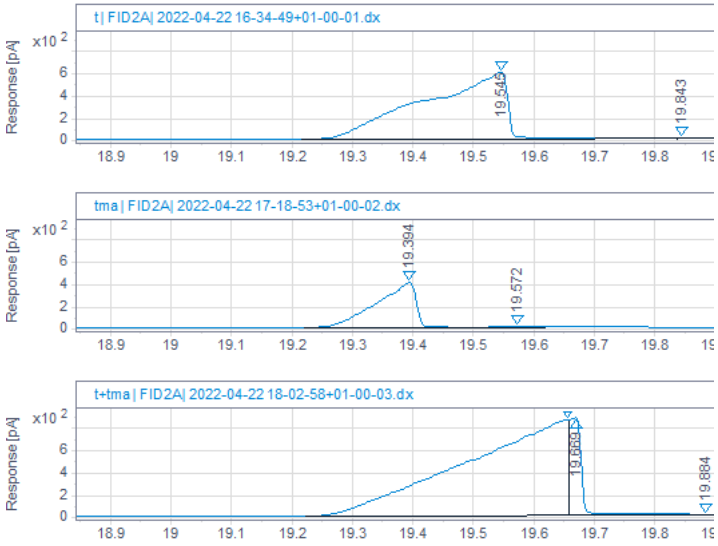

Figure 29- GC traces of 1)- 5-Methoxy-2-tetralone, 2) 5-Methoxy-*N*-methyl-1,2,3,4-tetrahydro-2-naphthaleneamine, 3) mixture of 5-methoxy-2-tetralone and 5-Methoxy-*N*-methyl-1,2,3,4-tetrahydro-2-naphthaleneamine in conditions of 100-140^{o}C with

each sample dissolved in ethyl acetate and with each sample run with a ramp rate of 5°C per min.

A similar result can also be observed in **Figure 30**, whereby both the ketone and aminated products were unable to give separate resolute peaks when mixed together. However, in each of the samples, the elution was at around 19 min.

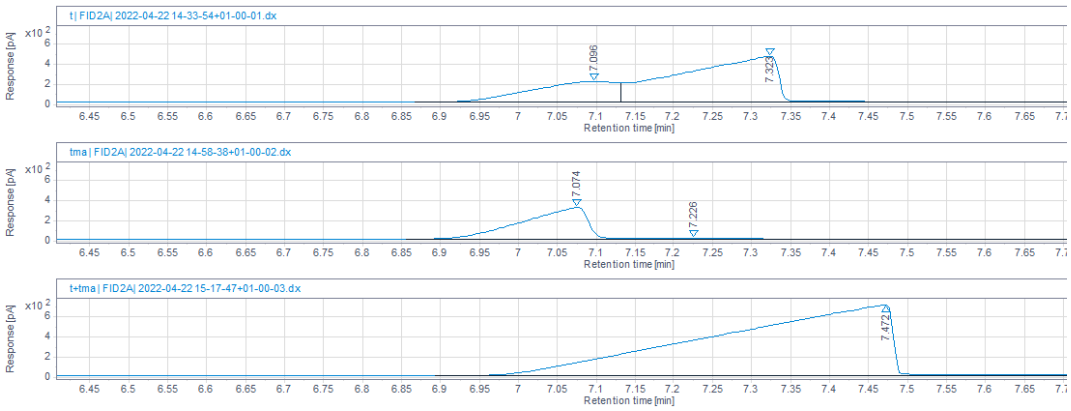

Figure 30- GC traces of 1) 5-Methoxy-2-tetralone, 2) 5-Methoxy-*N*-methyl-1,2,3,4-tetrahydro-2-naphthaleneamine standard, 3) mixture of 5-methoxy-2-tetralone and 5-Methoxy-*N*-methyl-1,2,3,4-tetrahydro-2-naphthaleneamine with each sample dissolved in ethyl acetate, and run in conditions of 140°C isothermal.

In the case of using 140°C isothermal, the ketone and aminated products eluted at around 7 min. Therefore, one can observe, neither of the traces showed two distinctive peaks with good resolution between the ketone and the aminated product. Hence, in the future more conditions can be tested to obtain the most optimal GC method for biotransformation studies with 5-Methoxy-2-tetralone.

3.5.2 Biotransformation studies with IR91

Having obtained the optimal GC condition for doing biotransformation studies with 2-tetralone and methylamine, catalyzed by 1 mg mL^{-1} of pure IR91, reactions were set up and assayed at several time points over 24 h. The $NADP^+$ cofactor recycling system was employed from the France *et al*. Samples were collected and quenched after 2h, 4h, 6h and 24h of the reaction. Each of the samples then subsequently underwent GC analysis. Using the ratio of the peaks between the 2-

tetralone and the respective product after reductive amination, product conversion was calculated after each time point and plotted to visualize the progression of the reaction. **Figure 31** shows the progressive changes of the GC trace (difference in peak height) as the reaction is carried out as well as a graph showing the increase in product conversion.

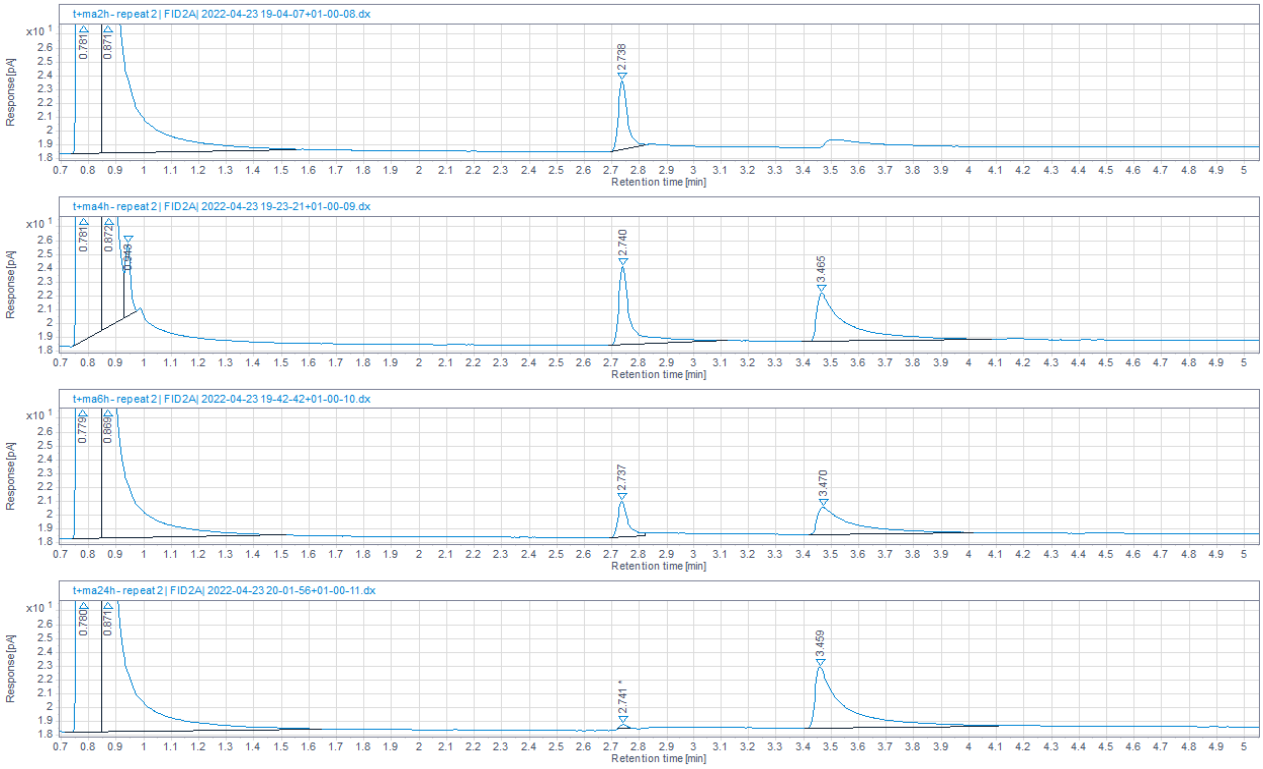

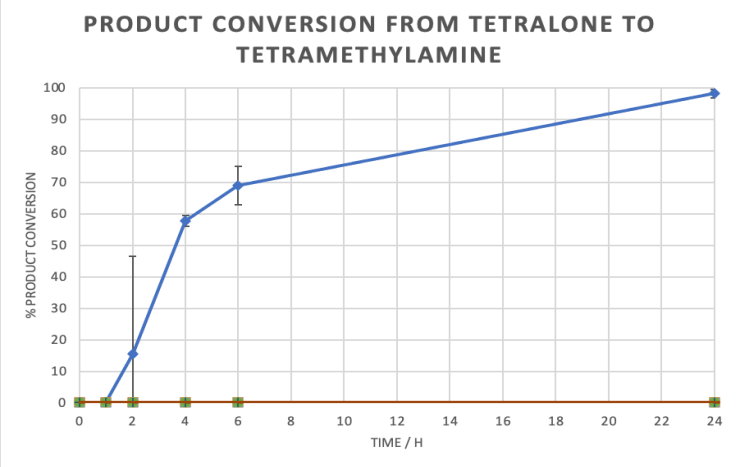

Figure 31- A) GC traces of reactions carried out between 5-methoxytetralone and methylamine, catalysed by IR91WT with samples collected at 2h, 4h, 6h, and 24h since the reaction. **B**) A graph showing product conversion from 2-tetralone to 2-tetramethylamine over a 24h time period.

From **Figure 31A** one can see the progressive decline of the height of the peak corresponding to 2-tetralone, which is around 2.7 min. This signals that the 2-tetralone is being transformed by the enzyme. In parallel, there is a progressive increase in the height of the peaks corresponding to the aminated product standard, at around 3.4 min. These are the same elution times as those established using the assay development test at 140ºC , shown in **Figure 27**. As a consequence, it indicates that the wild-type-IR91 enzyme is able to catalyze the reductive amination of 2-tetralone with methylamine.

4. Conclusions

The wild-type Imine Reductase IR91 was successfully expressed, purified and crystallized. From the crystals, a data set was produced and a structure of 1.35 Å resolution was solved, built and refined. The structure was in complex with $NADP^+$, showing high similarity to other IREDs, including RedAms. Owing to the absence of a ligand, crystal screens were again prepared by increasing the amount of 5-Methoxy-2-tetralone. As a result, a successful crystal structure of resolution 1.55 Å was also solved of WT-IR91 in complex with $NADP^+$ and 5-Methoxy-2-tetralone.

With the successfully expressed wild-type IR91, kinetic studies were carried out. After reducing the protein concentration, kinetic constants were produced for cyclohexanone. Valid kinetic constants were also produced with methylamine albeit with a large error. These can be used as a benchmark for mutant analysis. Kinetic analysis of mutants Y172A and S97A indicated that these had very poor activity, indicative of potentially significant roles in catalysis.

For carrying out biotransformation studies, assays were developed for analysing the reductive amination of 2-tetralone and 5-Methoxy-2-tetralone, with methylamine as the amine donor. Optimal GC conditions were tested in order to provide a benchmark for reaction analysis with these ketones and their respective aminated products. For 2-tetralone, a successful method was identified, while it was still more difficult to establish a method for 5-Methoxy-2-tetralone Using the optimal GC conditions, biotransformation studies with pure IR91 enzyme showed that it does

catalyse the reductive amination of 2-tetralone with methylamine with a very high product conversion of 98%.

Having obtained sufficient data for the wild-type of IR91, further work could include obtaining biotransformation data for mutants- Y172A, Y172F and S97A, of which the plasmids were already available. As previously mentioned, catalytic active site residues have been found to include leucine-180, tyrosine-172 and tryptophan. Using values from kinetic and biotransformation analysis, mutation of serine and tyrosine were performed and kinetic data was difficult to obtain.

The roles of Y172 and S97 can also be further assessed by carrying out biotransformation studies using these mutants in an attempt to compare to the benchmark values obtained using the wildtype. Additionally, mutations can be done on Leucine and Methionine, to study their effects on enzyme activity. These studies may help assess if there are any other potential residues affecting the substrate specificity and product conversion. Mutants with superior activity could then be used to scale up the synthesis of model compounds.

5-References

1. Afanasyev, O. I.; Kuchuk, E.; Usanov, D. L.; Chusov, D.; Reductive Amination in the Synthesis of Pharmaceuticals. *Chem Rev.* **2019,** *119*,11857-11911.
2. Ghislieri, D.; Turner, N. J.; Enantiomerically Pure Chiral Amines. *Top Catal.* **2014,** *57*, 284-300
3. Wang, C.; J, Xiao,; Stereoselective Formation of Amine. *Top. Curr. Chem.* **2014,** *343,* 261-282
4. Bodis, J.; Lefferts, L.; Muller, T.E.; Pestman, R.; Lercher, J.A.; Activity and selectivity control in reductive amination of butyraldehyde over noble metal catalysts. *Catal. Lett.* **2005,** *104,* 23-28
5. Bruer, M.; Ditrich, K.;, Habicher, T.; Hauer, B.; Keßeler, M.; Sturmer R.; Zelinski, T.; Industrial methods for the production of optically active intermediates. *Angew. Chem. Int. Ed. ,***2004***, 43,* 788-824

6. Huffman, M. A. et al. Design of an in vitro biocatalytic cascade for the manufacture of islatravir. *Science 366*, **2019**, 1255–1259
7. Gong, J.-S.; Lu, Z.-M.; Li, H.; Zhou, Z.-M.; Shi, J.-S.; Xu, Z.-H. Metagenomic Technology and Genome Mining: Emerging Areas for Exploring Novel Nitrilases. *Appl. Microbiol. Biotechnol.* **2013**, *97*, 6603– 6611, DOI: 10.1007/s00253-013-4932-8
8. Rosano, G. L.; Ceccarelli, E. A. Recombinant Protein Expression in *Escherichia coli*: Advances and Challenges. *Front. Microbiol.* **2014**, *5*, 1– 17, DOI: 10.3389/fmicb.2014.00172
9. Hammer, S. C.; Knight, A. M.; Arnold, F. H. Design and Evolution of Enzymes for Non-Natural Chemistry. *Curr. Opin. Green Sustain. Chem.* **2017**, *7*, 23– 30, DOI: 10.1016/j.cogsc.2017.06.002
10. Savile, C. K.; Janey, J. M.; Mundorff, J. C.; Moore, S. T.; Jarvis, W. R.; Colbeck, C.; Krebber, A.; Fleitz, F. J.; Brands, J.; Devine, P. N.; Huisman, G. W.; Hughes, G. J, Biocatalytic Asymmetric Synthesis of Chiral Amines from Ketones Applied to Sitagliptin. *Science, 329*, **2010**, 305-309
11. Arnold, F. H.; Combinatorial and computational challenges for biocatalyst design. *Nature.* **2001,** *409,* 253-257
12. Schoemaker, H. E.; Mink, D.; Wubbolts, M. G.; Dispelling the myths- biocatalysis in industrial synthesis. *Science.* **2003**, *299,* 1694-1697
13. Marin, A. R.; Disanto, R.; Plotnikov, I.; Kamat, S.; Shonnard, D.; Pannuri, S.; Improved activity and thermostability of (S)-aminotransferase by error-prone polymerase chain reaction for the production of chiral amine. *Biochem. Eng. J.* **2007***, 37,* 246-255
14. Ismali, H.; Lau, R. M.; Rantwijk, F. V.; Sheldon, R. A., Fully Enzymatic Resolution of Chiral Amines: Acylation and Deacylation in the Presence of *Candida antarctica* Lipase B, *Adv. Synth. Catal*. **2008**, *350*, 1511-1516
15. Balkenhohl, F.; Ditrich, K.; Hauer B.; Ladner, W.; Optically active amines via lipase-catalyzed methoxy acetylation. *J. Prakt. Chem.* **1997**, *339*, 381-38
16. Breuer, M.; Ditrich, K.; Habicher, T.l Hauer, B.; Keßeler, Sturmer, R.; Zelinski, T.; Industrial Methods for the Production of Optically Active Intermediates. *Angew. Chem. Int. Ed.* **2004**, *43*, 788-824
17. Mangion, I. K.; Sherry, B. D.; Yin, J. J.; Fleitz, F. J.; Enantioselective synthesis of Dual Orexin Receptor Antagonist. *Org. Lett. 14*, 2**012**, 3458-3461

18. Molinaro, C.; Bulger, P. G.; Lee, E. E.; Kosjek, B.; Lau, S.; Gauvreau, D.; Howard, M E.; Wallace, D. J.; O'Shea, P. D. CRTH2 Antagonist MK-7246: A Synthetic Evolution from Discovery through Development. *J. Org. Chem. 77*, **2012**, 2299-2309
19. Fuchs, M.; Koszelewski, D.; Tauber, K.; Sattler, J.; Banko, W.; Holzer, A. K.; Pickl, M.; Kroutil, W.; Faber, K.; Improved chemoenzymatic asymmetric synthesis of (*S*)-Rivastigmine. *Tetrahedron, 68,* **2012,** 7691-7694
20. Fuchs, M.; Koszelewski, D.; Tauber, K.; Kroutil, W.; Faber, K.; Chemoenzymatic asymmetric total synthesis of (*S*)-Rivastigmine using omega-transaminases. *Chem Commun, 46*, **2010**, 5500-5502
21. Busto, E.; Simon, C.; Grischeck, B.; Gotor-Fernandez, V.; Kroutil, W., Cutting Short the Asymmetric Synthesis of the Ramatroban Precursor by Employing ω-Transaminases, *Adv. Synth. Catal. 356*, **2014**, 1937-1942
22. Ohkubo, K.; Gotoh, M.; Effect of ramatroban, a thromboxane A_2 antagonist, in the treatment of perennial allergic rhitnis. *Allergol. Int.* 52, **2003**, 131-138
23. Farlow, M. R.; Cummings, J. L. Effective Pharmacologic Management of Alzheimer's Disease. *Am. J. Med. 120,* **2007,** 388-397
24. Emre, M.; Rivastigmine in Parkinson's Disease Dementia, *CNS Drugs, 20,* **2006**, 748
25. Kelly, S. A.; Mix, S.; Moody, T. S.; Gilmore, B. F.; Transaminases for industrial biocatalysis: novel enzyme discovery. *Appl. Microbiol. Biotechol. 104,* **2020**, 4781-4794
26. Maugeri, Z.; Rother, D.; Application of Imine Reductases (IREDs) in Micro-Aqueous reaction systems. *Adv. Synth. Catal.,* **2016,** *358,* 2745-2750
27. Montgomery, S. L.; Pushpanath, A.; Heath, R. S.; Marshall, J. R.; Klemstein, U.; Galman, J. L.; Woodlock, D.; Bisagni, S.; Taylor, C. J.; Mangaz-Sanchez, J.; Ramsden, J. I.; Dominguez, B.; Turner, N. J.; Characterization of imine reductases in reductive amination for the exploration of structure-activity relationships. *Adv Sci,* **2020,** *6*, 1-12
28. Alexeeva, M.; Enright, A.; Dawson, M. J.; Mahmoudian M.; Turner, N. J.; Deracemization of *α* -Methylbenzylamine Using an Enzyme Obtained by In Vitro Evolution. *Angew. Chem. Int. Ed.,* **2002,** *198*, 3177-3180
29. Carr, R.; Alexeeva, M.; Dawson, M. J.; Gotor-Fernandez, V.; Humphrey, C. E.; Turner, N. J.; Directed evolution of an amine oxdiase possessing both broad

substrate specificity and high enantioselectivity, *Angew. Chem. Int. Ed.,* **2003***, 42,* 4807-4810

30. Carr, R.; Alexeeva, M.; Dawson, M. J.; Gotor-Fernandez, V.; Humphrey, C. E.; Turner, N. J.; Directed evolution of an amine oxdiase for the preparative deracemization of racemization of cyclic secondary amines, *ChemBioChem,* **2005***, 6,* 637-639
31. Duan, J.; Li, B.; Qin, Y.; Dong, Y.; Ren, J.; Li, G. Recent progress in directed evolution of stereoselective monoamine oxidases. *Bioresour. Bioprocess.* **2019,** *6,* 1-11
32. Kohler, V.; Bailey, K. R.; Znabet, A.; Raftery, J.; Helliwell, M.; Turner, N. J., Enantioselective biocatalytic oxidative desymmetrization of substituted pyrrolidines. **2010**, *49*, 2182-2184
33. Revill, P.; Serradell, N.; Bolos, J.; Rosa, E, Telaprevir, *Drugs of the Future,* **2007**, *32*, 788-798
34. Njoroge, F. G.; Chen, K. V.; Shih, N-Y.; Piwinski, J. J. Challenges in modern drug discovery: a case study of boceprevir, an HCV protease inhibitor for the treatment of hepatitis C virus infection. *Acc. Chem. Res.* **2008**, *41*, 50-59
35. Leisch, H.; Grosse, S.; Iwaki, H.; Hasegawa, Y.; Peter, C. K.; Cyclohexylamine oxidase as a useful biocatalyst for the kinetic resolution and deracemization of amines. *Can. J. Chem.* **2011***, 90,* 31-45
36. Hohne, M.; Engineering imine reductases for industrial applications. *Nat. Catal.* **2019,** *2,* 841-842
37. Mangas-Sanchez, J.; Sharma. M.; Cosgrove, S. C.; Ramsden, J. I.; Marshall, J. R.; Thorpe, T. W.; Palmer, R. B.; Grogan, G.; Turner, N. J.; Asymmetric synthesis of primary amines catalyzed by thermotolerant fungal reductive aminases. *Chem Sci.* **2020,** *11,* 5052-5057
38. Maugeri, Z.; Rother, D.; Application of Imine Reductases (IREDs) in Micro-Aqueous Reaction Systems. *Adv. Synth. Catal.,* **2016** *358,* 2745-2750.
39. Mangas-Sanchez J., France S. P., Montgomery S. L., Aleku G. A., Man H., Sharma M., Ramsden J. I., Grogan G., Turner N. J., Imine Reductases, *Curr. Opin. Chem. Biol.* **2017**, *37*, 19–25.
40. Li, H.; Williams, P.; Micklefield, J.; Gardiner, J. M.; Stephens, G.; A dynamic combinatorial screen for novel imine reductase activity. *Tetrahedron,* **2004**, 60, 753-758

41. Wetzl, D.; Gand M.; Ross, A.; Muller, H.; Matzel, P.; Hanlon, S. P.; Muller, M.; Wirz B.; Hohne, M.; Iding H.; Asymmetric Reductive Amination of Ketones Catalyzed by Imine Reductases. *ChemCatChem* **2016,** *8* , 2023-2026
42. Matzel, P.; Wenske, S.; Merdivan, S.; Gunther, S.; Hohne, M.; Synthesis of β-Chiral Amines by Dynamic Kinetic Resolution of α-Branched Aldehydes Applying Imine Reductases. *ChemCatChem.* **2019,** *11* , 4281-4285.
43. Mitsukara, K.; Suzuki, M.; Shinoda, M.; Kuramoto, T.; Yoshida, T.; Nagasawa, T.; Purification and Characterization of a Novel (R)-Imine Reductase from *Streptomyces* sp. GF3587, **2011**, *75*, 1778-1782.
44. Rodriguez-Mata, M.; Frank, A.; Wells, E.; Leipold, F.; Turner, N. J.; Hart, S.; Turkenburg, J. P.; Grogan, G.; Structure and Activity of NADPH-Dependent Reductase Q1EQE0 from *Streptomyces kanamyceticus*, which Cataluses the *R*-Selective Reduction of an Imine Substrate, **2013,** *14,* 1372-1379.
45. Stockinger, P.; Roth, S.; Muller, M.; Pleiss, J.; Systematic Evaluation of Imine-Reducing Enzymes: Common Principles in Imine Reductases, beta-Hydroxy Acid dehydrogenases. *ChemBioChem,* **2020***, 21*, 2689-2695.
46. Huber, T.; Schneider, L.; Prag, A.; Gerhardt, S.; Einsle, O.; Muller, M.; Direct Reductive Amination of Ketones: Structure and Activity of S-Selective Imine Reductases from *Streptomyces*, *ChemCatChem*, **2014**, *6*, 2248-2252.
47. Scheller, P. N.; Lenz, M.; Hammer, S. C.; Hauer, B.; Nestl, B.; Nestl, B. M. Imine Reductase-Catalyzed Intermolecular Reductive Amination of Aldehydes and Ketones. *ChemCatChem,* **2015,** *7*, 3239-3242
48. Aleku, G. A.; France, P. S.; Man, H.; Mangas-Sanchez, J.; Montgomery, S. L.; Sharma, M.; Leipold, F.; Hussain, S.; Grogan, G.; Turner, N. J.; A reductive aminase from *Aspergillus oryzae*. *Nat. Chem.* **2017,** *9,* 961-969.
49. Sharma, M.; Mangas-Sanchez, J.; France, S. P.; Aleku, G. A.; Montgomery S. L.; Ramsden, J. I.; Turner, N.J.; Grogan, G.; A Mechanism for Reductive Amination Catalyzed by Fungal Reductive Aminases *ACS Catal.* **2018**, *8,* 11534-11541.
50. Zhang, L.; Chooback, L.; Cook, P. F.; Lysine 193 Is the General Base in the 6-Phosphogluconate Dehydrogenase-Catalyzed Reaction. *Biochemistry,* **1999,** *38,* 11231-11238.
51. France, S. P.; Howard, R. M.; Steflik, J.; Weise, N. J.; Mangas-Sanchez, J.; Montgomery, S. L.; Crook, R.; Kumar, R.; Turner, N. J.; Identification of Novel

Bacterial Members of the Imine Reductase Enzyme Family that Perform Reductive Amination, *ChemCatChem,* **2018**, *10,* 510-514

52. Man, H.; Wells, E.; Hussain, S.; Leipold, F.; Hart, S.; Turkenburg, J. P.; Turner, N. J.; Grogan, G., Structure, Activity and Stereoselectivity of NADPH-Dependent Oxidoreductases Catalysing the *S*-Selective Reduction of the Imine Substrate 2-Methylpyrroline, *ChemBioChem*, **2015**, *16*, 1052-1059
53. Roiban, G. D.; Kern, M.; Liu, Z.; Hyslop, J.; Tey, P. L.; Levine, M. S.; Jordan, J. S.; Brown, K. K.; Hadi, T.; Ihnken, L. A. F.; Brown, M. J. B., Efficient Biocatalytic Reductive Aminations by Extending the Imine Reductase Toolbox, *ChemCatChem*, **2017**, *9*, 4475-4479
54. Kabsch, W. XDS, *Acta Crystallogr. Sect. D Biol. Crystallogr.* **2010**, *66*, 125-132.
55. Evans, P. Scaling and Assessment of Data Quality, *Acta Crystallogr. Sect. D Biol. Crystallogr.,* **2006**, *62*, 72-82.
56. Winter, G. *xia2*: An Expert System for Macromolecular Crystallography Data Reduction, *J. Appl. Crystallogr.* **2010,** *43*, 186-190.
57. Vagin, A.; Teplyakov, A. MOLREP: An Automated Program for Molecular Replacement, *J. of Appl. Crystallogr.* **1997**, *30*, 1022-1025.
58. Emsley, P.; Cowtan, K., Coot: Model Building Tools for Molecular Graphics, *Acta Crystallogr. Sect. D Biol. Crystallogr.* **2004**, *60*, 2126-2132.
59. Murshudov, G. N.; Vagin, A. A.; Dodson, E. J. Refinement of Macromolecular Structures by the Maximum-Likelihood Method, *Acta Crystallogr. Sect. D Biol. Crystallogr.* **1997***, 53*, 240-255.
60. Ziegenhorn, J.; Senn, M.; Bucher, T.; Molar Absorptivities of beta-NADH and beta-NADPH, *Clin Chem*. **1976**, *22*, 151-160